EUROPEAN RESPIRATORY *journal*

FLAGSHIP SCIENTIFIC JOURNAL OF ERS

Early View

Original research article

Inhibition of MRTF activation as a clinically achievable anti-fibrotic mechanism for Pirfenidone

Hsiao-Yen Ma, Jason A. Vander Heiden, Salil Uttarwar, Ying Xi, Elsa-Noah N'Diaye, Ryan LaCanna, Patrick Caplazi, Sarah Gierke, John Moffat, Paul J. Wolters, Ning Ding

Please cite this article as: Ma H-Y, Vander Heiden JA, Uttarwar S, *et al*. Inhibition of MRTF activation as a clinically achievable anti-fibrotic mechanism for Pirfenidone. *Eur Respir J* 2022; in press (https://doi.org/10.1183/13993003.00604-2022).

Inhibition of MRTF activation as a clinically achievable anti-fibrotic mechanism for Pirfenidone

Hsiao-Yen Ma[1], Jason A. Vander Heiden[2], Salil Uttarwar[2], Ying Xi[1*], Elsa-Noah N'Diaye[1**], Ryan LaCanna[1], Patrick Caplazi[3***], Sarah Gierke[3], John Moffat[4], Paul J. Wolters[5], Ning Ding[1****]

1 Department of Discovery Immunology, Genentech, South San Francisco, CA, USA.

2 Department of OMNI Bioinformatics, Genentech, South San Francisco, CA, USA.

3 Department of Pathology, Genentech, South San Francisco, CA, USA.

4 Department of Biochemical and Cellular Pharmacology, Genentech, South San Francisco, CA, USA

5 Department of Medicine, University of California, San Francisco, CA, USA.

* Current address: School of Life Science and Technology, ShanghaiTech University, 201210 Shanghai, China.

** Current address: Gilead Sciences, Foster City, CA, USA.

*** Current address: AbbVie, South San Francisco, CA, USA.

**** e-mail: ding.ning@gene.com

Idiopathic pulmonary fibrosis (IPF) is a progressive fibrotic disease characterized by aberrant fibroblast/myofibroblast accumulation and excessive collagen matrix deposition in the alveolar areas of lungs. As the first approved IPF medication, pirfenidone (PFD) significantly decelerates lung function decline while its

underlying anti-fibrotic mechanism remains elusive. In this study, using transcriptomic and immunofluorescence analyses of primary human IPF tissues, we showed that myocardin related transcription factor (MRTF) signaling is activated in myofibroblasts accumulated in IPF lungs. Furthermore, we showed that PFD inhibits MRTF activation in primary human lung fibroblasts at the clinically achievable concentrations (half-maximal inhibitory concentration (IC_{50})=50-150uM, maximal inhibition>90%, maximal concentration of PFD in patients<100uM). Mechanistically, PFD appears to exert its inhibitory effects by promoting the interaction between MRTF and actin indirectly. Finally, PFD-treated IPF lungs exhibit significantly less MRTF activation in FF areas than naïve IPF lungs. Our results suggest MRTF signaling as a direct target for PFD and implicate that some of the anti-fibrotic effects of PFD may be due to MRTF inhibition in lung fibroblasts.

Introduction

Idiopathic pulmonary fibrosis (IPF) is a progressive and fatal interstitial lung disease with a median survival of 3–5 years after diagnosis[1-4]. Although the underlying pathobiology of IPF is complex and poorly understood, it is proposed that the disease is likely triggered by repetitive microinjuries to the airway and alveolar epithelium[5]. These parenchymal insults lead to the activation and accumulation of myofibroblasts in interstitial areas of lungs. Consequently, these myofibroblasts synthesize and deposit excessive amounts of extracellular matrix (ECM) proteins into alveolar regions, which

results in progressive lung function decline and, ultimately, patient death[6,7]. Therefore, IPF represents a huge unmet medical need for the global public health system[5-8].

Numerous experimental therapies have failed in clinical trials of IPF and, to date, only two medications have been approved for the treatment of IPF patients: pirfenidone (PFD) and nintedanib (NTD), based on their ability to slow disease progression as measured by reduced lung function decline[9,10]. While NTD has been proposed to target fibroblast and myofibroblast proliferation and activation as a potent multiple receptor tyrosine kinase (RTK) inhibitor[11,12], the anti-fibrotic mechanism of PFD remains elusive. In this regard, it should be noted that recent studies have linked PFD to a wide spectrum of biological activities such as targeting profibrotic growth factors and transcription factors, inhibiting collagen fibril formation, and antagonizing oxidative stress [13-18]. However, the limitation of these studies is the use of the excessive concentrations of PFD and/or the lack of human evidence. Thus, the clinical relevance of these observations has not been fully established and the molecular target(s) for PFD in patients are yet to be defined[19,20].

The serum response factor (SRF) is an important transcription factor that regulates cytoskeleton and cell motility gene expression via the interaction with its two main coactivators, myocardin related transcription factor A and B (MRTFA/B)[21-26]. In unstimulated cells, MRTFA is largely sequestered in cytoplasm by binding to monomeric actin (G-actin) via its N-terminal arginine-proline-glutamate-leucine consensus sequence containing (RPEL) domain[23,27-29]. When cells are stimulated, ras homolog

(RHO) GTPases are activated to trigger polymerization of G-actin to filamentous actin (F-actin), thereby releasing MRTFs from G-actin and allowing them to be predominantly translocated into the nucleus to induce cytoskeleton gene expression via interaction with SRF[23,27-29]. The critical role of MRTF signaling in cell motility and cytoskeleton reprogramming is further supported by human genetics data that MRTFA loss-of-function mutation causes immune susceptibility to viral infections and aberrant wound healing response due to compromised motility of immune cells and fibroblasts[17]. Mouse studies have also demonstrated that MRTF signaling contributes to tissue fibrosis in multiple preclinical models[30-36].

Here, we hypothesize that certain dysregulated molecular pathway(s) in human IPF lungs may be targeted by PFD for its anti-fibrotic action. Using transcriptomic analyses of human samples, we found that MRTF signaling is induced in human IPF lungs and its hyperactivation appears to be specific to mesenchymal cells including fibroblasts and myofibroblasts. Furthermore, the complementary immunofluorescence analysis revealed that MRTF activation appears to be mainly derived from α-smooth muscle actin (ACTA2) expressing myofibroblasts accumulated in IPF lungs. Next, we showed that PFD inhibits MRTFA nuclear translocation, a central cellular event of MRTF signaling activation, and MRTF target gene expression in a dose-dependent manner. The potency of PFD on antagonizing MRTF signaling was further experimentally determined as the half-maximal inhibitory concentration (IC_{50})=50-150uM and maximal inhibition>90%. Mechanistically, we observed that PFD promotes the interaction between MRTF and actin indirectly without impacting ras homolog family member A

(RHOA) activation and actin polymerization. Consistent to these findings, PFD-treated but not NTD-treated IPF lungs exhibit less MRTF activation in FF than those in naïve IPF lungs without PFD treatment. In sum, these data suggest MRTF signaling as a direct molecular pathway that can be inhibited by PFD at the physiologically relevant concentrations, which may represent a new and clinically achievable anti-fibrotic mechanism for the drug.

Results

MRTF signature is enriched in IPF lungs

In order to advance our understanding of the pathobiology of human lung fibrosis, we performed genome-wide transcriptomic analysis on freshly explanted human lungs from patients with IPF and non-diseased controls[37]. In parallel, transcriptional profiles were also collected from mesenchymal cells isolated directly from the same lungs via triple negative ($CD45^-EPCAM^-CD31^-$) sorting (Figures 1A and S1). Gene ontology (GO) analysis revealed that biological processes such as cell projection represented by cilium-associated genes and cell movement were among top upregulated processes in IPF lungs, which is consistent with previous reports[38-43] (Figure 1B). In addition, cytoskeleton and its related cell motility pathways were also enriched in the upregulated genes from IPF lungs (Figure 1B). We then sought to determine whether enrichment of cytoskeleton and motility genes was caused by dysregulation of gene expression in mesenchymal cells or, alternatively, by aberrant accumulation of mesenchymal cell populations such as fibroblasts/myofibroblasts in fibrotic lungs. Upon cell sorting, we found that cytoskeleton and cell motility were still among the top upregulated biological

processes in sorted IPF mesenchymal cells (Figure 1B), suggesting enrichment of these processes is likely due to transcriptional changes rather than imbalances in cellularity.

To identify underlying transcriptional conduits responsible for cytoskeleton and motility gene expression, we explored potential transcription factors that may contribute to cytoskeleton and motility reprogramming by using Molecular Signatures Database (MSigDB)[44] and found that SRF putative target genes are highly enriched in cytoskeleton and motility genes upregulated in IPF lungs among top hits (Figure 1C). As SRF stimulate motility and cytoskeleton gene expression via MRTFs[21-24],[25,26], we next aimed to determine if MRTF signaling is hyperactive in fibrotic lungs by generating a MRTF response signature to measure its activity. The distribution of relative expression for MRTF response signature (IPF versus non-diseased lungs) displayed a marked shift compared to that of all other genes analyzed (Figure 1D). Unsupervised clustering analysis of non-diseased controls and IPF patients using the same MRTF signature showed a separation between non-fibrotic and fibrotic samples (Figures 1E, F). We also performed a similar analysis of MRTF signature in another previously reported IPF cohort [45]. Consistently, we found a significant enrichment of MRTF signature in IPF lungs when compared to healthy controls (Figures S2A-C). Thus, the observations from two independent IPF cohorts support the hyperactivation of MRTF signaling in IPF lungs.

MRTF activation in myofibroblasts in IPF lungs

To investigate the cellular source of MRTF activation, we performed the immunofluorescence assays to examine the MRTFA nuclear localization, a molecular

hallmark of MRTF activation, in IPF lungs. In this regard, we observed a prominent MRTFA nuclear localization in ACTA2+ myofibroblasts accumulated in the fibroblast foci (FF), a histological feature of IPF lungs (Figures 2A, E). It should also be noted that diffuse MRTFA signal was observed in both cytoplasm and nuclei in EPCAM+ epithelial cells (Figures 2B, E), implicating less MRTF activation in these cells than that in myofibroblasts. On the other hand, we only found negligible cytoplasmic and nuclear MRTFA signal in CD31+ endothelial cells and CD45+ immune cells (Figures 2C, D and E). Therefore, these results suggest that myofibroblasts may be the main cell type that mediates MRTF activation in IPF lungs.

PFD inhibits MRTF activation in a clinically relevant dose range in lung fibroblasts

The hyperactivation of MRTF signaling in IPF lung mesenchymal cells, particularly (myo)fibroblasts, prompts us to speculate that PFD may target this pathway to achieve, at least, some of its anti-fibrotic actions. Therefore, to test this possibility, we examined whether PFD could inhibit serum-induced MRTFA nuclear translocation in two independent primary human lung fibroblast lines isolated from normal and IPF human lungs respectively. As expected, PFD attenuated serum-induced MRTFA nuclear translocation in a dose-dependent manner without compromising the overall MRTFA protein level (Figures 3A and C). In addition, we did not observe any significant impact of PFD on fibrillar collagen gene expression and lung fibroblast viability (Figures S2 and S3) and, consistently, a latest report suggested that MRTF signaling is not required for these two processes in fibroblasts[46]. The IC_{50} for PFD on MRTF nuclear translocation is

~100uM and ~150uM for each fibroblast line with the maximal inhibition reaching above 90% (Figures 3B, D, E). Notably, the IC_{50} of PFD to inhibit MRTFA nuclear translocation is in the range of its clinically observed concentrations (<100uM)[47-49], suggesting that partial inhibition of MRTF signaling may be achievable for PFD in human IPF patients. We also determined the impact of PFD on MRTF activation in non-fibroblastic cells such as alveolar epithelial cells, immune cells (e.g. neutrophils, macrophages, dendritic cells) and lung artery endothelial cells. The data showed that PFD exhibits little effect on serum-induced MRTF activation in those cell types even at the concentration of 1mM (Figure S4), indicating that PFD may selectively inhibit MRTF signaling in lung fibroblasts.

Transcriptomic analysis of the inhibitory effects of PFD on MRTF signaling in lung fibroblasts

Next, we sought to evaluate the systemic impact of PFD on the transcriptional response of serum-induced MRTF signaling in lung fibroblasts. We chose 1mM PFD for this experiment as this is the concentration that PFD can achieve 90% or more MRTF inhibition in both lung fibroblast lines tested. RNA-seq analysis of serum stimulated primary human lung fibroblasts revealed that PFD suppressed a series of MRTF direct target genes (Figures 4A and S5A). Consistently, GO analysis of PFD downregulated genes showed a significant functional enrichment for MRTF-related categories including cell adhesion, cell motility, migration and cell morphogenesis (Figures 4B and S5B).

In addition to activating MRTF signaling, serum can strongly stimulate other pathways such as ternary complex factor (TCF)[50] and Hippo signaling[51]. So, if PFD selectively targeted MRTF signaling, we would expect no significant impact of PFD on TCF or Hippo downstream target gene expression. To this end, we compared several well-established TCF and Hippo target gene expression stimulated by serum in the absence or presence of PFD. As expected, we observed no significant effects of PFD on those gene expression (Figures 4A, D, E and S5A). Furthermore, PFD appears to suppress serum-induced MRTF target gene (e.g. *ACTA2* and *MYL9*) expression through MRTFA as depletion of MRTFA completely abolishes PFD's antagonistic effects (Figures 4F-H), supporting the specificity of PFD as an MRTF inhibitor.

To further investigate if these findings are clinically relevant, we determined the PFD dose responsive curve of two MRTF target genes, *ACTA2* and *MYL9*. In agreement with its inhibitory activity on MRTFA nuclear translocation (Figure 3E), PFD exhibits the similar potency on suppression of serum-induced *ACTA2* and *MYL9* expression: IC_{50} ranges between 50 and 150uM and the maximal inhibition is more than 90% (Figures 5A-C). Taken together, these results suggest that PFD is a selective inhibitor of MRTF signaling in lung fibroblasts, at least, *in vitro*.

PFD promotes the binding of MRTF to actin indirectly

As we observed the inhibitory effects of PFD on MRTF signaling, an intriguing question arises: what could be the mechanistic bases underlying its activity against MRTF? In this regard, we considered the following three key upstream cellular events of MRTF

nuclear translocation that may be affected by PFD: 1. Rho GTPase/ ras homolog family member A (RHOA) activation; 2. actin polymerization; 3. MRTF-actin interaction.

First, we explored whether PFD inhibits serum-induced RHOA activation and we observed no significant impact of 1mM PFD in RHOA activation (Figure 6A). Similarly, we found 1mM PFD does not affect G-actin polymerization into F-actin induced by serum while Latrunculin B (LanB), a well-documented actin polymerization inhibitor, can dramatically disrupt this process (Figure 6B). Finally, we tested the possibility that PFD may modulate the physical interaction between MRTF and actin. We fused the actin binding domain of MRTFA, RPEL domain, (2-261) with 6xHis tag (His-RPEL) and performed pull-down assays by incubating this recombinant fusion protein with the cytoplasmic extract from lung fibroblasts treated with or without PFD at the indicated concentrations. The results showed that PFD increases the recruitment of endogenous actin to His-RPEL recombinant protein in a dose-dependent manner (Figure 6C). To determine whether PFD promotes this interaction directly, we repeated the pulldown assays in a reconstituted system consisting of recombinant His-RPEL fusion protein and purified actin protein, instead of cell extracts, in the presence or absence of 1mM PFD. The result showed that PFD does not enhance the interaction between RPEL and actin in this reconstituted system even at the concentration of 1mM (Figure 6D). Collectively, these data suggest that PFD is likely to promote MRTF/actin physical interaction in an indirect manner, which may serve as the molecular basis of PFD’s antagonistic action on MRTF signaling.

PFD attenuates MRTF nuclear localization in FF of IPF lungs

While our data establish PFD as an MRTF inhibitor *in vitro*, the evidence to support MRTF signaling as a clinically achievable target for PFD in human IPF patients is lacking. To this end, we analyzed the subcellular localization of MRTFA in the FF regions found in a cohort comprising IPF patients treated with or without PFD or NTD[52]. Quantification of MRTFA immunoreactivity demonstrated that the nuclear MRTFA signal in FF is significantly lower in IPF patients treated with PFD than that in IPF patients untreated with PFD (Figures 7A, B). Conversely, we observed that the cytoplasmic MRTFA signal in FF is significantly higher in IPF patients treated with PFD than that in IPF patients untreated with PFD (Figures 7A, B). Additionally, we determined the subcellular localization of MRTFA in FF in IPF patients treated with NTD from the same cohort and found no significant change when compared to untreated IPF patients (Figures 7A, B). In support of this observation, we did not find any impact of NTD (1uM) on MRTF target gene expression in lung fibroblasts *in vitro* either (Figure S6). On the other hand, we also noticed that neither PFD nor NTD affects MRTFA nuclear/cytoplasmic distribution in EPCAM+ epithelial cells in IPF lungs (Figure S7), supporting the notion that PFD may specifically antagonize MRTF activation in lung fibroblasts and myofibroblasts. In sum, these data suggest that PFD, but not NTD, inhibits *in situ* MRTF activation in human IPF lungs.

Discussion

Within the past few decades, the biomedical community has cured tissue fibrosis many times in animals. However, only PFD, as well as NTD, exhibits clinical benefits in IPF

patients[9,10]. Thus, it is of utmost importance to understand how these medications work to benefit IPF patients. Herein, we, for the first time, establish MRTF signaling as a clinically relevant and achievable target for PFD. This finding is supported by a series of quantitative analyses of PFD's inhibitory effects on MRTF signaling both *in vitro* and *in situ*. In an *in vitro* fibroblast culture system, we measured the inhibitory potency of PFD on MRTF signaling using two complementary readouts: MRTFA nuclear accumulation and MRTF target gene expression. The data from these independent experiments consistently indicate that the IC_{50} of PFD against MRTF signaling ranges between 50-150uM and the maximal inhibition is more than 90%. To our knowledge, this is the first potency profile of PFD to be reported. More importantly, we presented the human data that PFD attenuates MRTF signaling by ~30% in IPF lungs. Considering that the clinically achievable concentration for PFD is less than 100uM in patients[47-49], we propose that PFD is a clinically relevant inhibitor of MRTF signaling in patients.

The molecular basis of PFD's antagonistic action on MRTF signaling was also investigated in the current study. As the main biological activity of PFD is to inhibit MRTF nuclear accumulation, we thoroughly explored whether PFD may modulate the upstream cellular events of this process. To our surprise, we found that PFD appears to promote the interaction between MRTF and actin indirectly without impacting RHOA activation and actin polymerization. Then, what could be the direct molecular targets of PFD? In this regard, because actin is embedded in a complex cytoskeleton network, it is logical to speculate that PFD may target certain molecular interface(s)/conduit(s) within the cytoskeleton network to modulate MRTF/actin interaction indirectly (Figure 7C). This

possibility may also help explain the selective effect of PFD on MRTF activation in fibroblasts as the cytoskeleton, a central determinant of cell shape and morphology, is the only subcellular structure that distinguishes fibroblasts from the other cell types[53,54]. Nonetheless, additional studies are needed to fully delineate the direct action site(s) of PFD within the actin/cytoskeleton network in fibroblasts.

The anti-fibrotic action of PFD has often been linked to its anti-inflammatory and anti-fibrotic activities against pathways such as transforming growth factor β (TGFβ), tumor necrosis factor α (TNFα) and p38 signaling[14,55-57]. However, the main caveat in most studies is the use of the excessive and clinically unachievable concentrations (mostly at the mM concentration range) of PFD to demonstrate its activity against these pathways. From a pharmacological point of view, the antagonistic activity of PFD on these pathways may be clinically irrelevant and may not contribute to PFD's therapeutic efficacy in patients. In support of this notion, recent studies reported that TGFβ signaling was not affected by PFD in patient samples [15,52]. Thus, it is in this context that our finding that establishes PFD as an MRTF inhibitor at the clinically achievable concentrations bridges the gap of PFD's pharmacological activity between bench side and bedside. On the other hand, since MRTF signaling is a critical regulator of mechanotransduction[22,28,29] and the emerging evidence suggests mechanical stress as a key driver of lung fibrosis progression[58,59], it is possible that PFD's antagonistic action on MRTF signaling might contribute to its therapeutic efficacy.

The major adverse events of PFD in patients include rash, gastrointestinal events, decrease in body weight and elevation of the level of alanine or aspartate aminotransferase (ALT/AST) in livers[9,60]. However, MRTF deficiency in both human and mouse has not been reported to be linked to these safety liabilities[23,61,62]. One explanation for this discrepancy is that mechanisms underlying PFD's side effects may be independent from its anti-fibrotic activity. Given the chemical nature of small molecules, it is plausible that PFD could modulate targets other than MRTF signaling to exert its adverse effects in patients. Future studies are therefore warranted to explore non-MRTF targets for PFD, which may enable potential modifications of PFD to improve its therapeutic index in patients.

Up to 45% of deaths in the developed world can be attributed to progressive fibrotic diseases[5]. However, till recently, the development of safe and efficacious anti-fibrotic therapies has been confounded by our poor understanding of the molecular drivers of fibrosis progression in patients. Thus, our current study that establishes PFD as a clinically relevant MRTF inhibitor may not only shed a light on the puzzling anti-fibrotic mechanism of PFD but also illuminate MRTF signaling as a druggable driver of chronic fibrosis progression.

Reference

1 Kim, D. S., Collard, H. R. & King, T. E., Jr. Classification and natural history of the idiopathic interstitial pneumonias. *Proc Am Thorac Soc* **3**, 285-292, doi:10.1513/pats.200601-005TK (2006).

2 Flaherty, K. R. *et al.* Clinical significance of histological classification of idiopathic interstitial pneumonia. *Eur Respir J* **19**, 275-283, doi:10.1183/09031936.02.00182002 (2002).

3 King, T. E., Jr. *et al.* Idiopathic pulmonary fibrosis: relationship between histopathologic features and mortality. *Am J Respir Crit Care Med* **164**, 1025-1032, doi:10.1164/ajrccm.164.6.2001056 (2001).

4 Nicholson, A. G., Colby, T. V., du Bois, R. M., Hansell, D. M. & Wells, A. U. The prognostic significance of the histologic pattern of interstitial pneumonia in patients presenting with the clinical entity of cryptogenic fibrosing alveolitis. *Am J Respir Crit Care Med* **162**, 2213-2217, doi:10.1164/ajrccm.162.6.2003049 (2000).

5 Wynn, T. A. & Ramalingam, T. R. Mechanisms of fibrosis: therapeutic translation for fibrotic disease. *Nat Med* **18**, 1028-1040, doi:10.1038/nm.2807 (2012).

6 Coward, W. R., Saini, G. & Jenkins, G. The pathogenesis of idiopathic pulmonary fibrosis. *Ther Adv Respir Dis* **4**, 367-388, doi:10.1177/1753465810379801 (2010).

7 Raghu, G. *et al.* Idiopathic pulmonary fibrosis in US Medicare beneficiaries aged 65 years and older: incidence, prevalence, and survival, 2001-11. *Lancet Respir Med* **2**, 566-572, doi:10.1016/S2213-2600(14)70101-8 (2014).

8 Collard, H. R. *et al.* Health care utilization and costs of idiopathic pulmonary fibrosis in U.S. Medicare beneficiaries aged 65 years and older. *Ann Am Thorac Soc* **12**, 981-987, doi:10.1513/AnnalsATS.201412-553OC (2015).

9 King, T. E., Jr. *et al.* A phase 3 trial of pirfenidone in patients with idiopathic pulmonary fibrosis. *N Engl J Med* **370**, 2083-2092, doi:10.1056/NEJMoa1402582 (2014).

10 Richeldi, L. *et al.* Efficacy and safety of nintedanib in idiopathic pulmonary fibrosis. *N Engl J Med* **370**, 2071-2082, doi:10.1056/NEJMoa1402584 (2014).

11 Hilberg, F. *et al.* BIBF 1120: triple angiokinase inhibitor with sustained receptor blockade and good antitumor efficacy. *Cancer Res* **68**, 4774-4782, doi:10.1158/0008-5472.CAN-07-6307 (2008).

12 Wollin, L. *et al.* Mode of action of nintedanib in the treatment of idiopathic pulmonary fibrosis. *Eur Respir J* **45**, 1434-1445, doi:10.1183/09031936.00174914 (2015).

13 Macias-Barragan, J., Sandoval-Rodriguez, A., Navarro-Partida, J. & Armendariz-Borunda, J. The multifaceted role of pirfenidone and its novel targets. *Fibrogenesis Tissue Repair* **3**, 16, doi:10.1186/1755-1536-3-16 (2010).

14 Conte, E. *et al.* Effect of pirfenidone on proliferation, TGF-beta-induced myofibroblast differentiation and fibrogenic activity of primary human lung fibroblasts. *Eur J Pharm Sci* **58**, 13-19, doi:10.1016/j.ejps.2014.02.014 (2014).

15 Knuppel, L. *et al.* A Novel Antifibrotic Mechanism of Nintedanib and Pirfenidone. Inhibition of Collagen Fibril Assembly. *Am J Respir Cell Mol Biol* **57**, 77-90, doi:10.1165/rcmb.2016-0217OC (2017).

16 Didiasova, M. *et al.* Pirfenidone exerts antifibrotic effects through inhibition of GLI transcription factors. *FASEB J* **31**, 1916-1928, doi:10.1096/fj.201600892RR (2017).
17 Ruwanpura, S. M., Thomas, B. J. & Bardin, P. G. Pirfenidone: Molecular Mechanisms and Potential Clinical Applications in Lung Disease. *Am J Respir Cell Mol Biol* **62**, 413-422, doi:10.1165/rcmb.2019-0328TR (2020).
18 Xi, Y. *et al.* The anti-fibrotic drug pirfenidone inhibits liver fibrosis by targeting the small oxidoreductase glutaredoxin-1. *Sci Adv* **7**, eabg9241, doi:10.1126/sciadv.abg9241 (2021).
19 Iyer, S. N. *et al.* Dietary intake of pirfenidone ameliorates bleomycin-induced lung fibrosis in hamsters. *J Lab Clin Med* **125**, 779-785 (1995).
20 Raghu, G., Johnson, W. C., Lockhart, D. & Mageto, Y. Treatment of idiopathic pulmonary fibrosis with a new antifibrotic agent, pirfenidone: results of a prospective, open-label Phase II study. *Am J Respir Crit Care Med* **159**, 1061-1069, doi:10.1164/ajrccm.159.4.9805017 (1999).
21 Miano, J. M., Long, X. & Fujiwara, K. Serum response factor: master regulator of the actin cytoskeleton and contractile apparatus. *Am J Physiol Cell Physiol* **292**, C70-81, doi:10.1152/ajpcell.00386.2006 (2007).
22 Olson, E. N. & Nordheim, A. Linking actin dynamics and gene transcription to drive cellular motile functions. *Nat Rev Mol Cell Biol* **11**, 353-365, doi:10.1038/nrm2890 (2010).
23 Record, J. *et al.* Immunodeficiency and severe susceptibility to bacterial infection associated with a loss-of-function homozygous mutation of MKL1. *Blood* **126**, 1527-1535, doi:10.1182/blood-2014-12-611012 (2015).
24 Esnault, C. *et al.* Rho-actin signaling to the MRTF coactivators dominates the immediate transcriptional response to serum in fibroblasts. *Genes Dev* **28**, 943-958, doi:10.1101/gad.239327.114 (2014).
25 Tschumperlin, D. J., Ligresti, G., Hilscher, M. B. & Shah, V. H. Mechanosensing and fibrosis. *J Clin Invest* **128**, 74-84, doi:10.1172/JCI93561 (2018).
26 Lighthouse, J. K. & Small, E. M. Transcriptional control of cardiac fibroblast plasticity. *J Mol Cell Cardiol* **91**, 52-60, doi:10.1016/j.yjmcc.2015.12.016 (2016).
27 Miralles, F., Posern, G., Zaromytidou, A. I. & Treisman, R. Actin dynamics control SRF activity by regulation of its coactivator MAL. *Cell* **113**, 329-342, doi:10.1016/s0092-8674(03)00278-2 (2003).
28 Gau, D. & Roy, P. SRF'ing and SAP'ing - the role of MRTF proteins in cell migration. *J Cell Sci* **131**, doi:10.1242/jcs.218222 (2018).
29 Small, E. M. The actin-MRTF-SRF gene regulatory axis and myofibroblast differentiation. *J Cardiovasc Transl Res* **5**, 794-804, doi:10.1007/s12265-012-9397-0 (2012).
30 Li, Z. *et al.* MKL1 promotes endothelial-to-mesenchymal transition and liver fibrosis by activating TWIST1 transcription. *Cell Death Dis* **10**, 899, doi:10.1038/s41419-019-2101-4 (2019).
31 Mao, L. *et al.* MKL1 mediates TGF-beta-induced CTGF transcription to promote renal fibrosis. *J Cell Physiol* **235**, 4790-4803, doi:10.1002/jcp.29356 (2020).
32 Shiwen, X. *et al.* A Role of Myocardin Related Transcription Factor-A (MRTF-A) in Scleroderma Related Fibrosis. *PLoS One* **10**, e0126015, doi:10.1371/journal.pone.0126015 (2015).

33 Yu-Wai-Man, C., Treisman, R., Bailly, M. & Khaw, P. T. The role of the MRTF-A/SRF pathway in ocular fibrosis. *Invest Ophthalmol Vis Sci* **55**, 4560-4567, doi:10.1167/iovs.14-14692 (2014).
34 Bernau, K. *et al.* Megakaryoblastic leukemia-1 is required for the development of bleomycin-induced pulmonary fibrosis. *Respir Res* **16**, 45, doi:10.1186/s12931-015-0206-6 (2015).
35 Small, E. M. *et al.* Myocardin-related transcription factor-a controls myofibroblast activation and fibrosis in response to myocardial infarction. *Circ Res* **107**, 294-304, doi:10.1161/CIRCRESAHA.110.223172 (2010).
36 Fan, Z. *et al.* MKL1 is an epigenetic modulator of TGF-beta induced fibrogenesis. *Biochim Biophys Acta* **1849**, 1219-1228, doi:10.1016/j.bbagrm.2015.07.013 (2015).
37 DePianto, D. J. *et al.* Molecular mapping of interstitial lung disease reveals a phenotypically distinct senescent basal epithelial cell population. *JCI Insight* **6**, doi:10.1172/jci.insight.143626 (2021).
38 Selman, M. *et al.* Accelerated variant of idiopathic pulmonary fibrosis: clinical behavior and gene expression pattern. *PLoS One* **2**, e482, doi:10.1371/journal.pone.0000482 (2007).
39 Yang, I. V. *et al.* Expression of cilium-associated genes defines novel molecular subtypes of idiopathic pulmonary fibrosis. *Thorax* **68**, 1114-1121, doi:10.1136/thoraxjnl-2012-202943 (2013).
40 Ahluwalia, N. *et al.* Fibrogenic Lung Injury Induces Non-Cell-Autonomous Fibroblast Invasion. *Am J Respir Cell Mol Biol* **54**, 831-842, doi:10.1165/rcmb.2015-0040OC (2016).
41 Tager, A. M. *et al.* The lysophosphatidic acid receptor LPA1 links pulmonary fibrosis to lung injury by mediating fibroblast recruitment and vascular leak. *Nat Med* **14**, 45-54, doi:10.1038/nm1685 (2008).
42 Geng, Y. *et al.* PD-L1 on invasive fibroblasts drives fibrosis in a humanized model of idiopathic pulmonary fibrosis. *JCI Insight* **4**, doi:10.1172/jci.insight.125326 (2019).
43 Li, Y. *et al.* Severe lung fibrosis requires an invasive fibroblast phenotype regulated by hyaluronan and CD44. *J Exp Med* **208**, 1459-1471, doi:10.1084/jem.20102510 (2011).
44 Xie, X. *et al.* Systematic discovery of regulatory motifs in human promoters and 3' UTRs by comparison of several mammals. *Nature* **434**, 338-345, doi:10.1038/nature03441 (2005).
45 Sivakumar, P. *et al.* RNA sequencing of transplant-stage idiopathic pulmonary fibrosis lung reveals unique pathway regulation. *ERJ Open Res* **5**, doi:10.1183/23120541.00117-2019 (2019).
46 Xi, Y. *et al.* A WISP1 antibody inhibits MRTF signaling to prevent the progression of established liver fibrosis. *Cell Metabolism*, doi:10.1016/j.cmet.2022.07.009 (2022).
47 Wollin L, S. J., Ostermann A. The effect of nintedanib compared to pirfenidone on serum-stimulated proliferation of human primary lung fibroblasts at clinically relevant concentrations. *Am J Respir Crit Care Med* **191**, A4940 (2015).
48 Shi, S. *et al.* Single- and multiple-dose pharmacokinetics of pirfenidone, an antifibrotic agent, in healthy Chinese volunteers. *J Clin Pharmacol* **47**, 1268-1276, doi:10.1177/0091270007304104 (2007).

49 Rubino, C. M., Bhavnani, S. M., Ambrose, P. G., Forrest, A. & Loutit, J. S. Effect of food and antacids on the pharmacokinetics of pirfenidone in older healthy adults. *Pulm Pharmacol Ther* **22**, 279-285, doi:10.1016/j.pupt.2009.03.003 (2009).

50 Treisman, R. Ternary complex factors: growth factor regulated transcriptional activators. *Curr Opin Genet Dev* **4**, 96-101, doi:10.1016/0959-437x(94)90097-3 (1994).

51 Yu, F. X. *et al.* Regulation of the Hippo-YAP pathway by G-protein-coupled receptor signaling. *Cell* **150**, 780-791, doi:10.1016/j.cell.2012.06.037 (2012).

52 Zhang, Y. *et al.* Histopathological and molecular analysis of idiopathic pulmonary fibrosis lungs from patients treated with pirfenidone or nintedanib. *Histopathology* **74**, 341-349, doi:10.1111/his.13745 (2019).

53 Tarin, D. & Croft, C. B. Ultrastructural features of wound healing in mouse skin. *J Anat* **105**, 189-190 (1969).

54 Kalluri, R. & Zeisberg, M. Fibroblasts in cancer. *Nat Rev Cancer* **6**, 392-401, doi:10.1038/nrc1877 (2006).

55 Schaefer, C. J., Ruhrmund, D. W., Pan, L., Seiwert, S. D. & Kossen, K. Antifibrotic activities of pirfenidone in animal models. *Eur Respir Rev* **20**, 85-97, doi:10.1183/09059180.00001111 (2011).

56 Oku, H., Nakazato, H., Horikawa, T., Tsuruta, Y. & Suzuki, R. Pirfenidone suppresses tumor necrosis factor-alpha, enhances interleukin-10 and protects mice from endotoxic shock. *Eur J Pharmacol* **446**, 167-176, doi:10.1016/s0014-2999(02)01757-0 (2002).

57 Nakazato, H., Oku, H., Yamane, S., Tsuruta, Y. & Suzuki, R. A novel anti-fibrotic agent pirfenidone suppresses tumor necrosis factor-alpha at the translational level. *Eur J Pharmacol* **446**, 177-185, doi:10.1016/s0014-2999(02)01758-2 (2002).

58 Wu, H. *et al.* Progressive Pulmonary Fibrosis Is Caused by Elevated Mechanical Tension on Alveolar Stem Cells. *Cell* **180**, 107-121 e117, doi:10.1016/j.cell.2019.11.027 (2020).

59 Herrera, J., Henke, C. A. & Bitterman, P. B. Extracellular matrix as a driver of progressive fibrosis. *J Clin Invest* **128**, 45-53, doi:10.1172/JCI93557 (2018).

60 Noble, P. W. *et al.* Pirfenidone in patients with idiopathic pulmonary fibrosis (CAPACITY): two randomised trials. *Lancet* **377**, 1760-1769, doi:10.1016/S0140-6736(11)60405-4 (2011).

61 Sun, Y. *et al.* Acute myeloid leukemia-associated Mkl1 (Mrtf-a) is a key regulator of mammary gland function. *Mol Cell Biol* **26**, 5809-5826, doi:10.1128/MCB.00024-06 (2006).

62 Li, S., Chang, S., Qi, X., Richardson, J. A. & Olson, E. N. Requirement of a myocardin-related transcription factor for development of mammary myoepithelial cells. *Mol Cell Biol* **26**, 5797-5808, doi:10.1128/MCB.00211-06 (2006).

63 Ware, L. B. *et al.* Assessment of lungs rejected for transplantation and implications for donor selection. *Lancet* **360**, 619-620, doi:10.1016/s0140-6736(02)09774-x (2002).

64 Pau G, R. J. HTSeqGenie: A NGS analysis pipeline. *R package* (2013).

65 Srinivasan, K. *et al.* Untangling the brain's neuroinflammatory and neurodegenerative transcriptional responses. *Nat Commun* **7**, 11295, doi:10.1038/ncomms11295 (2016).

66 Law, C. W., Chen, Y., Shi, W. & Smyth, G. K. voom: Precision weights unlock linear model analysis tools for RNA-seq read counts. *Genome Biol* **15**, R29, doi:10.1186/gb-2014-15-2-r29 (2014).

67 Wu, D. & Smyth, G. K. Camera: a competitive gene set test accounting for inter-gene correlation. *Nucleic Acids Res* **40**, e133, doi:10.1093/nar/gks461 (2012).
68 Subramanian, A. *et al.* Gene set enrichment analysis: a knowledge-based approach for interpreting genome-wide expression profiles. *Proc Natl Acad Sci U S A* **102**, 15545-15550, doi:10.1073/pnas.0506580102 (2005).
69 Team, R. C. R: A language and environment for statistical computing. *R Foundation for Statistical Computing, Vienna, Austria* **https://www.R-project.org** (2018).
70 Ding, N. *et al.* Mediator links epigenetic silencing of neuronal gene expression with x-linked mental retardation. *Mol Cell* **31**, 347-359, doi:10.1016/j.molcel.2008.05.023 (2008).

Acknowledgements We thank the Genentech histology and FACS laboratories for technical assistance; the Genentech Center for Advanced Light Microscopy for imaging; and the Genentech NGS lab for RNA-seq. We also thank Linda Rangell and Debra Dunlap for immunohistochemistry support.

Author contributions H.Y.M. designed the study, performed the experiments, analyzed the data, and wrote the manuscript; J.A.V.H., S.U. performed analysis of RNAseq data and contributed to the data interpretation; Y.X., R.L., E.N-D performed the experiments; P.C. contributed to the histological analysis of fibrotic tissues; S.G. helped with immunofluorescence imaging; P.J.W. provided human lung explants and IPF lung biopsies; N.D. designed the study, performed the experiments, analyzed the data, wrote the manuscript with H.Y.M. and supervised the study.

Figure Legends

Figure 1. MRTF signature is enriched in IPF lungs.

(**A**) Schematic overview of human sample collection. (**B**) Top GO biological processes enriched in genes upregulated in fibrotic samples. (**C**) Top 10 cis-regulatory motifs enriched in the promoter regions of upregulated cytoskeleton and cell motility genes in IPF lungs. (**D**) Density fit of $\log_2$ fold-change distributions of IPF vs normal lungs. Separate distributions are shown for MRTF response genes (MRTF signature) and all other genes with expression levels passing quality control (Background). The displayed density fit is truncated at the bounds of the observed $\log_2$fold-change values within each category of genes. MRTF signature ≠ Background. (**E**) Violin plot of MRTF signature in normal and IPF lungs (Normal lungs, n = 4; IPF lungs, n = 10). (**F**) Unsupervised hierarchical clustering analysis of MRTF signature gene expression in IPF (n = 10) and normal lungs (n = 4). p value is calculated using unpaired two-tailed t-test.

Figure 2. Activation of MRTF signaling in myofibroblasts of IPF lungs

(**A**-**D**) Representative immunofluorescence images of MRTFA co-stained with ACTA2 (**A**), EPCAM (**B**), CD31 (**C**) and CD45 (**D**) in IPF lung sections. Arrowhead, nuclear MRTFA in ACTA2+ myofibroblasts. (**E**) Quantification of nuclear and cytoplasmic MRTFA fluorescent signal normalized by cell numbers in ACTA2+, EPCAM+, CD45+ and CD31+ cells in IPF lungs. (IPF samples (n=10) were used for MRTFA signal quantification in EPCAM+, CD45+ and CD31+ cells, and IPF samples (n=8) were used for MRTFA signal in ACTA2+ cells due to the lack of FFs in 2 IPF samples.) Data represents mean ± S.D.

Figure 3. PFD inhibits serum-induced MRTFA nuclear accumulation in hLFs at the clinically relevant concentrations.

(**A**, **C**) Representative western blot of nuclear (top panel) and whole cell extract (WCE) (bottom panel) MRTFA in human normal (**A**) and IPF (**C**) lung fibroblasts, treated with 20% fetal bovine serum (FBS) in the absence or presence of PFD at the indicated concentrations. Ying Yang 1 (YY1), loading control for nuclear fractions. Glyceraldehyde-3-phosphate dehydrogenase (GAPDH), loading control for WCE. (**B**, **D**) Quantification of nuclear accumulation of MRTFA in normal (**A**) and IPF (**C**) lung fibroblasts. (**E**) Summary of PFD potency on nuclear MRTFA accumulation. Data in E represents mean ± standard deviation (SD) of three independent experiments. p value is calculated FBS vs FBS+PFD using one-way ANOVA. *: $p < 0.05$. **: $p < 0.01$. $^{\#}$: $p < 0.0001$. ns; not significant.

Figure 4. Transcriptomic analysis of PFD inhibitory effects on MRTF signaling.

(**A**) Heatmap showing relative expression of MRTF, TCF and Hippo target genes in normal human lung fibroblasts treated with or without PFD. (**B**) Top GO biological processes enriched in the genes suppressed by PFD in 20% FBS stimulated normal human lung fibroblasts. (**C-E**) qPCR validation of PFD inhibition on MRTF target gene (**C**), TCF (**D**) and Hippo (**E**) target gene expression in normal and IPF human lung fibroblasts. (**F**-**G**) *ACTA2* and *MYL9* expression in SFM or 20% FBS stimulated normal (**F**) and IPF (**G**) human lung fibroblasts transfected with MRTFA or control siRNA in the presence or absence of PFD. (**H**) Representative western blot of MRTFA in WCE from SFM or 20% FBS stimulated human normal and IPF lung fibroblasts transfected with

MRTFA or control siRNA in the presence or absence of PFD. GAPDH, loading control for whole cell extracts. PFD concentration: 1mM, n = 3 biological replicates. p value is calculated using one-way ANOVA. * indicates comparison of SFM vs FBS, # indicates comparison of FBS vs FBS+PFD. *, #: $p < 0.05$. **, ##: $p < 0.01$. ***, ###: $p < 0.001$.

Figure 5. Determination of PFD inhibitory potency on MRTF target gene expression in hLFs.

(**A**, **B**) Dose-response curve of PFD inhibition on MRTF target gene expression in human normal (**A**) and IPF (**B**) lung fibroblasts. (**C**) Summary of PFD inhibitory potency on MRTF target gene expression. Data in **C** represents mean ± standard deviation (SD) of three independent experiments, n=3 biological replicates. p value is calculated FBS vs FBS+PFD using one-way ANOVA. *: $p < 0.05$. **: $p < 0.01$. #: $p < 0.0001$. ns; not significant.

Figure 6. PFD promotes MRTFA and actin interaction indirectly

(**A**) RHOA activation in human lung fibroblasts stimulated with 20% FBS in the absence or presence of PFD at the indicated concentrations, n=3 biological replicates. (**B**) F-actin formation in human lung fibroblasts stimulated with 20% FBS in the absence or presence of 1mM PFD or 100nM Latrunculin B (LanB), n=3 biological replicates. (**C**) Top panel: the His-RPEL fusion protein was used to immobilize endogenous actin in cytoplasmic lysates isolated from FBS-stimulated human lung fibroblasts treated with PFD at the indicated concentrations followed by actin WB. Bottom panel: coomassie blue staining of membrane showing His-RPEL fusion proteins used in the pulldown

assays. (**D**) Top panel: the His-RPEL fusion protein was used to immobilize purified actin in the absence or presence of 1mM PFD followed by actin WB. Bottom panel: Coomassie blue staining of membrane showing His-RPEL fusion proteins used in the pulldown assays. Data in **C** and **D** are representative and similar results were seen in three independent experiments. p value is calculated using one-way ANOVA. **, $p < 0.01$. ****, $p < 0.01$. ns, not significant.

Figure 7. PFD inhibits MRTF activation in human IPF lungs

(**A**) Representative images of MRTFA immunofluorescence signal in FF regions of naÏve and PFD or NTD treated IPF lung sections, scale bar 20μm. Arrowhead, nuclear MRTFA in ACTA2+ myofibroblasts. (**B**) Nuclear/cytoplasmic distribution of MRTFA in ACTA2+ myofibroblasts accumulated within FF regions (n=8 for IPF, n=9 for PFD-treated, n=8 for NTD-treated, certain samples are excluded due to the lack of FF). (**C**) Schematic summary of the proposed mechanism of PFD's inhibitory activity on MRTF pathway. Data represents mean ± standard deviation (SD) error. p value is calculated using one-way ANOVA. **, $p < 0.01$.

Figure S1. Flow sorting strategy for human lung mesenchymal cells.

(**A**) Representative flow plot showing sorting strategy and percentage of populations in normal human lungs. (**B**) COL1A1, EPCAM and CD31 expression in freshly sorted mesenchymal cells ($CD45^-EPCAM^-CD31^-$), epithelial cells ($EPCAM^+$) and endothelial cells ($CD31^+$) from normal and IPF lungs.

Figure S2. Enrichment of MRTF signature in a larger IPF cohort.

(**A**) Density fit of $\log_2$ fold-change distributions of IPF vs normal lungs. Separate distributions are shown for MRTF response genes (MRTF signature) and all other genes with expression levels passing quality control (Background). The displayed density fit is truncated at the bounds of the observed $\log_2$fold-change values within each category of genes. $p < 0.0001$, MRTF signature ≠ Background. (**B**) Violin plot of MRTF signature in normal and IPF lungs (Normal lungs, n = 26; IPF lungs, n = 46). p value is calculated using one-way ANOVA. (**C**) Unsupervised hierarchical clustering analysis of MRTF signature gene expression in IPF (n = 46) and normal lungs (n = 26).

Figure S3. PFD does not affect collagen expression and cell viability in hLFs.

(**A**) RT-qPCR validation of PFD inhibition on COL1A1, COL1A2 and COL3A1 expression in normal and IPF human lung fibroblasts. (**B**) Normal and IPF lung fibroblasts were treated with PFD at the indicated concentrations for 48 hours followed by CellTiter-Glo assay. PFD concentration: 1mM, n = 3 biological replicates.

Figure S4. PFD does not inhibit serum induced MRTFA nuclear translocation in non-fibroblastic cells.

(**A**-**F**) Representative western blot of MRTFA in WCE (top panel) and nuclear fractions (bottom panel) in A549 cells (**A**), MLE12 mouse alveolar epithelial cells (**B**), HL60-derived neutrophil-like cells (**C**), THP1-derived DC-like cells (**D**), U937-derived macrophage-like cells (**E**) and primary human lung artery endothelial cells (**F**) under indicated conditions. PFD concentration: 1mM. YY1, loading control for nuclear

fractions. β-actin, loading control for WCE. Similar results were seen in three independent experiments.

Figure S5. Transcriptomic analysis of PFD inhibitory effects on MRTF signaling in IPF LFs.

(**A**) Heatmap showing relative expression of MRTF, TCF and Hippo target genes in IPF human lung fibroblasts treat with or without 1mM PFD. n = 3/group. (**B**) Top GO biological processes enriched in the genes suppressed by PFD in 20% FBS stimulated IPF human lung fibroblasts.

Figure S6. NTD does not inhibit serum induced MRTF target gene expression in hLFs.

MRTF target gene expression in normal and IPF lung fibroblasts treated with DMSO, PFD (1mM) or NTD (1μM) in the presence or absence of 20% FBS. n = 3 biological replicates.

Figure S7. Neither PFD nor NTD impacts MRTF activation in EPCAM+ epithelial cells in human IPF lungs.

(**A**) Representative images of MRTFA and EPCAM immunofluorescence signal in naÏve and PFD- or NTD-treated IPF lung sections, scale bar 20μm. (**B**) Nuclear/cytoplasmic distribution of MRTFA in EPCAM+ epithelial cells (n=10 for IPF, n=10 for PFD-treated, n=10 for NTD-treated). Data represents mean ± standard deviation (SD) error. Statistical analysis using one-way ANOVA. ns, not significant.

Materials and Methods

Patient cohort. All human sample acquisitions were approved by the UCSF institutional review board. The clinical profile and demographic information of IPF patients and healthy control subjects are listed in Table S1. The IPF patient cohort treated with or without PFD or NTD has been reported before[52]. In this cohort, the mean duration of PFD treatment is 22.7 months (range = 9-60 months) and the mean duration of NTD treatment is 13.4 months (range = 7-20 months)[52].

Human lung samples. Explanted lung tissues were obtained from patients with a pathologic diagnosis of usual interstitial pneumonia and a consensus clinical diagnosis of IPF assigned by multidisciplinary discussion and review of clinical materials. Written informed consent was obtained from all subjects and the study was approved by the UCSF institutional review board. Human lungs not used by the Northern California Transplant Donor Network were used as controls; studies indicate that these lungs are physiologically and pathologically normal[63]. After perfusion of the pulmonary arteries and bronchoalveolar lavage, fresh lung explant tissue was stored in complete media on wet ice overnight before subsequent digestion. IPF lung biopsies treated with or without PFD or NTD were described previously[52].

Primary human lung cell isolation. The tissue was washed in HBSS and then thoroughly minced in digestion buffer (HBSS, 2.5mg/mL Collagenase D, 100µg/mL DNase). Minced tissue was rocked 45 minutes at 37°C. Residual tissue material was

transferred into fresh digestion buffer and rocked another 45 minutes at 37°C. Single cells from both rounds of digest were combined and then filtered through 70µm and 40µm strainers. Red blood cells were removed using Red Blood Cell Lysis Buffer (Sigma-Aldrich). The cell preparations were stained with anti-human CD45-BUV395 (1:250, BD Biosciences, #563792), anti-human EPCAM PE (1:250, BioLegend, #324206), anti-human CD31 PerCP-Cy5.5 (1:250, BioLegend, #303132), Fixable Viability Dye eFluor™ 780 (1:2000, ThermoFisher Scientific, #650-0865-14) and FACS sorted for $EPCAM^{pos}$, $CD31^{pos}$, $CD45^{pos}$ and triple negative populations using BD FACSAria™ and analyzed with Flowjo™.

Cell culture. A539, U937, MLE12, HL60 and THP1 cells were purchased from ATCC. Primary human lung artery endothelial cells were purchased from ScienCell. These primary cells were cultured as instructed by vendors. Primary hLFs were isolated from crude whole lung single-cell suspension and cultured in Dulbecco's Modified Eagle Medium (DMEM) supplemented with 2mM L-glutamine, 100 U/ml penicillin, 100 µg/ml streptomycin and 10% FBS. U937 cells were differentiated into macrophage-like cells by 20 ng/mL phorbol-12-myristate-13-acetate (PMA) (Cayman Chemical, Ann Arbor, Michigan, USA) treatment for 24 hours prior to SFM starvation and FBS stimulation. HL60 cells were differentiated into neutrophil-like cells by 1.5% v/v DMSO treatment for 6 days prior to SFM starvation and FBS stimulation. THP1 cells were differentiated into DC-like cells by 20 ng/mL of IL-4 (R&D Systems, Minneapolis, Minnesota, USA) and 20 ng/mL of PMA for 4 days prior to SFM starvation and FBS stimulation.

RNA-sequencing. RNA from lung fibroblasts were extracted using RNeasy kit (Qiagen) and treated with DNaseI (Life Technologies). The libraries were generated with Illumina TruSeq Stranded mRNA kit and were sequenced on HiSeq 2500 in high output mode.

RNA-seq analysis. Sequencing reads for both lung data published herein and previously published liver data (ENA accession ERP109255) were filtered and aligned using HTSeqGenie v3.4.1[64]. GSNAP v2011-12-28 was used for alignment, through the HTSeqGenie wrapper, against the GENCODE Basic gene model on the human genome assembly GRCh38. Only reads with unique genomic alignments were analyzed.

nRPKM (normalized Reads Per Kilobase gene model per Million total reads) values were used as a normalized measure of gene expression, calculated as previously defined[65]. Log_2 nRPKM transformations were calculated on nRPKM+1^{-4}, and the Z-scored log_2 nRPKM ranges displayed in the heatmaps were restricted to $\pm$ 3 standard deviations of the log_2 nRPKM values for visualization purposes; heatmap clustering was performing using Ward's method. Differential gene expression was calculated using voom+limma[66] with multiple-hypothesis correction of p-values performed using the Benjamini-Hochberg method. Significance tests of the MRTF response gene set compared to background where performed using the parametric camera method on the log-fold change distributions[67].

For differential gene expression and gene ontology analysis, upregulated genes were defined as genes having an nRPKM fold change > 0, and adjusted p-value < 0.05.

Gene ontology (GO) analysis was performed using the MSigDB gene sets[68]. The MRTF response signature was derived from the overlap between previously reported MRTF direct target genes[24] and cytoskeleton or motility-related genes upregulated in IPF lungs. Log_2 nRPKM fold-change distributions include all MRTF response genes against all other genes (background), excluding genes which did not have at least 10 reads in at 10% of the samples. Sample signature scores for the MRTF response gene set where defined as the first principal component score of a PCA analysis calculated on the log_2 nRPKM of the MRTF response gene set (eigengene). All RNA-seq analyses were conducted in R[69].

Immunofluorescence staining. 4µm sections of formalin-fixed and paraffin embedded specimens were deparaffinated followed by antigen retrieval using Target Retrieval (Dako #S1700). The sections were subsequently blocked and stained in PBS plus 1% BSA (Gibco), 5% nonimmune donkey serum (Jackson Immuno Research) and 0.1% Triton X-100. The following primary antibodies were used for IF: anti-MRTFA (1:100; Sigma-Aldrich, #HPA030782), anti-ACTA2-FITC (1:250; Sigma-Aldrich, #F3777), anti-EPCAM (1:500; Cell Signaling Technology, #2929), anti-CD45 (1:400; Cell Signaling Technology, #55618), anti-CD31 (1:1000; Cell Signaling Technology, #3528). Human sections were imaged with a 20x Plan Apo DIC M objective (NA: 0.75, Nikon) on a Nikon Ti-Eclipse inverted microscope equipped with an Andor Neo scMOS camera (Andor, Oxford Instruments), a linear-encoded automated stage (Applied Scientific Instrumentation), and a SOLA LED light engine (Lumencor) all run by NIS Elements software (Nikon).

Transfection of siRNAs. Transfection was carried out at a concentration 20nM of indicated siRNAs (Horizon Discovery) using RNAiMax transfection reagent (Thermo Fisher). Transfected cells were cultured without perturbation for at least 48 h prior to SFM starvation and 20% FBS stimulation.

RT-qPCR. Cultured primary human normal and IPF LFs were starved with serum-free medium (SFM) for overnight and then treated with 20% FBS and PFD or NTD at the indicated concentrations for another 24hrs. Subsequently, cells were harvested for RNA extraction. Total RNA was purified using RNeasy kit (Qiagen) and treated with DNaseI (Life Technologies). Complementary DNA synthesis was carried out with iScript RT Supermix (Bio-Rad). Quantitative PCR was performed in technical triplicates using SYBR Green reagent (Bio-Rad). The relative standard curve method was used for quantitation and expression levels were calculated by normalization to HPRT.

Western blot. Western blot was carried out whole cell extracts or nuclear extracts as previously described[70]. Equal amounts of protein lysates were separated by SDS–PAGE, transferred to a nitrocellulose membrane, and subjected to immunoblotting analysis using following primary antibodies: MRTFA (1:200, Santa Cruz, #32909), YY1 (1:1000, Abcam, #109237), GAPDH (1:1000, CST, #5174), ACTB (1:200, Santa Cruz, #sc-47778).

Cell-based functional assays. For proliferation assay, primary human lung fibroblasts cultured in 96-well plates were treated with PFD at the indicated concentrations for 48 h followed by CellTiter-Glo assay (Promega). For RHOA activation assay, primary human lung fibroblasts were starved in serum-free medium (SFM) for 24 h then treated with 20% FBS plus PFD at the indicated concentrations for 2 h and intracellular RHOA activity was measured using RHOA G-LISA Activation Assay Kit (Cytoskeleton). For F-actin formation assay, primary human lung fibroblasts starved in SFM for 24 h were treated with 20% FBS plus PFD (1mM) or LanB (100nM) for 2 h followed by fixation in 4% paraformaldehyde, permeabilization in 0.1% saponin and staining with 0.33µM rhodamine phalloidin solution in a sequential order. Cells were then thoroughly washed, and bound phalloidin was extracted by 30 min incubation with pure methanol. F-actin content was determined by measuring rhodamine phalloidin fluorescence using 537 nm for excitation and 576 nm for emission.

Pulldown assays. For pulldown assays using cell extracts, Ni-NTA agarose (Thermo) was saturated with 6xHis peptides or His-RPEL fusion protein from *Escherichia coli* lysates, washed, and used as affinity resin, which was subsequently incubated with cytoplasmic extracts from primary human lung fibroblasts, generated by lysis in hypotonic buffer (10mM HEPES [pH=7.9], 10mM KCl, 1.5mM $MgCl_2$, 0.1mM dithiothreitol [DTT] and protease inhibitors) through syringing and removal of insoluble material by centrifugation. An equivalent of a confluent 10-cm dish of primary human lung fibroblasts was used for one binding reactions. For pulldown assays in a reconstituted system, affinity resin saturated with 6xHis peptides or His-RPEL protein

were incubated with purified actin protein (Cytoskeleton Inc.) instead of cytoplasmic extracts from primary human lung fibroblasts. Binding reactions in both assays were for 2h in the binding buffer (50mM Tris-HCl [pH=7.5], 250mM NaCl, 1mM $MgCl_2$, 0.2mM ATP, 0.1mM DTT and protease inhibitors), supplemented with 0.5% TX-100. The resin was then washed three times in the binding buffer without protease inhibitors and subjected to 4 to 20% SDS-PAGE. The high molecular weight (>25 Kd) section of the gel was used for actin WB (4970; Cell Signaling) and the low molecular weight (<25 Kd) section of the gel was Coomassie blue stained to reveal bait input.

Quantification and Statistical Analysis

Custom scripts in R v3.5.1 were utilized for RNA-seq data analysis and plotting. GraphPad Prism was utilized for plotting and statistical analysis. Statistical details of experiments can be found in figure legends, including the statistical tests used and value and definition of n.

Data and Code Availability

RNA-seq data will be available before publication. Further information about sample preparation, data collection, or data processing is described in the method details and can also be directed to the Lead Contact.

Declaration of interests

All authors except Paul J. Wolters are or were employees of Genentech.

Figure 1

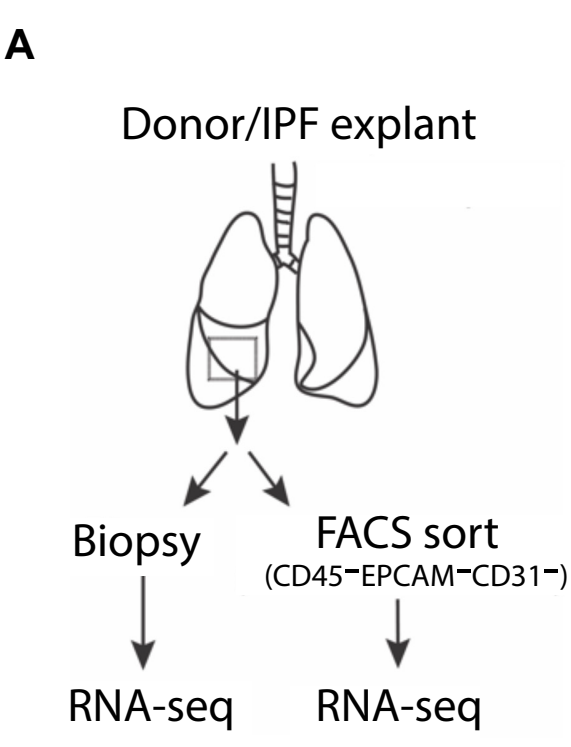
A
Donor/IPF explant
Biopsy
FACS sort
(CD45⁻EPCAM⁻CD31⁻)
RNA-seq
RNA-seq

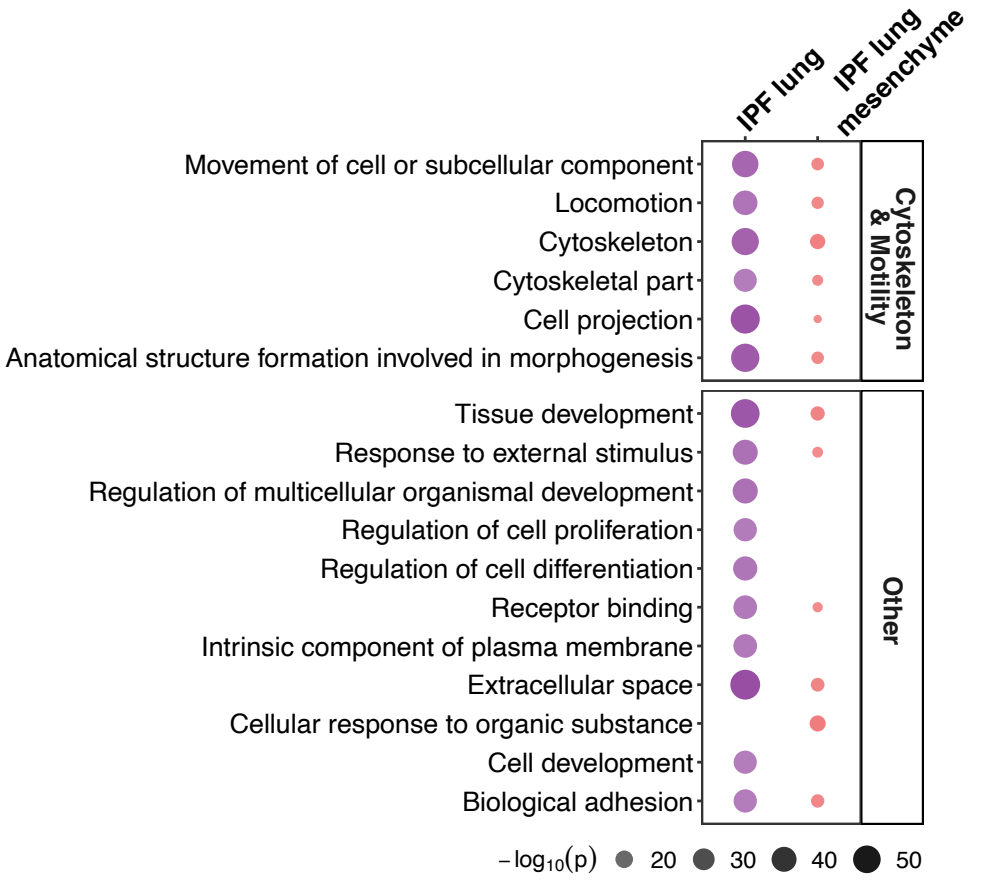
B
IPF lung
IPF lung mesenchyme
Movement of cell or subcellular component
Locomotion
Cytoskeleton
Cytoskeletal part
Cell projection
Anatomical structure formation involved in morphogenesis
Cytoskeleton & Motility
Tissue development
Response to external stimulus
Regulation of multicellular organismal development
Regulation of cell proliferation
Regulation of cell differentiation
Receptor binding
Intrinsic component of plasma membrane
Extracellular space
Cellular response to organic substance
Cell development
Biological adhesion
Other
−log10(p) 20 30 40 50

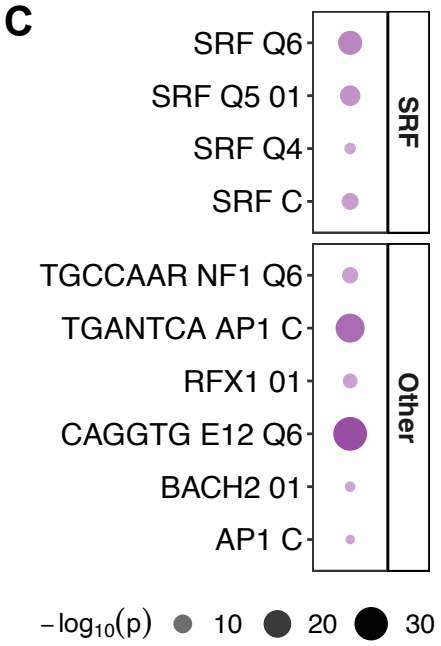
C
SRF Q6
SRF Q5 01
SRF Q4
SRF C
SRF
TGCCAAR NF1 Q6
TGANTCA AP1 C
RFX1 01
CAGGTG E12 Q6
BACH2 01
AP1 C
Other
−log10(p) 10 20 30

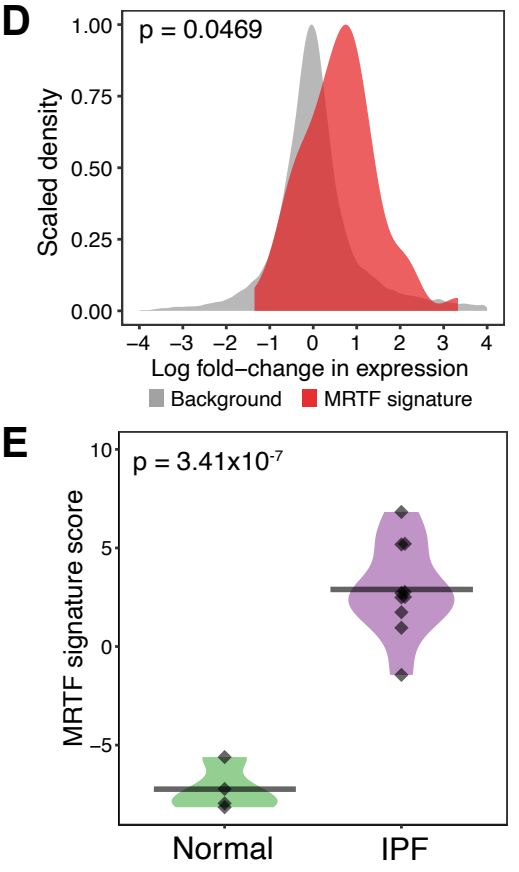
D
p = 0.0469
Scaled density
Log fold−change in expression
Background
MRTF signature
E
p = 3.41x10-7
MRTF signature score
Normal
IPF

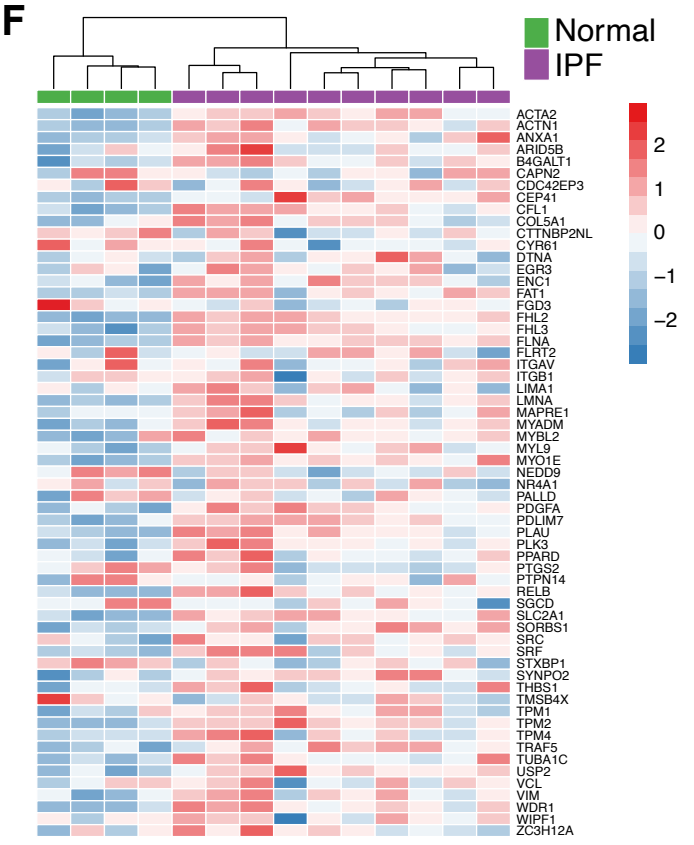
F
Normal
IPF
ACTA2
ACTN1
ANXA1
ARID5B
B4GALT1
CAPN2
CDC42EP3
CEP41
CFL1
COL5A1
CTTNBP2NL
CYR61
DTNA
EGR3
ENC1
FAT1
FGD3
FHL2
FHL3
FLNA
FLRT2
ITGAV
ITGB1
LIMA1
LMNA
MAPRE1
MYADM
MYBL2
MYL9
MYO1E
NEDD9
NR4A1
PALLD
PDGFA
PDLIM7
PLAU
PLK3
PPARD
PTGS2
PTPN14
RELB
SGCD
SLC2A1
SORBS1
SRC
SRF
STXBP1
SYNPO2
THBS1
TMSB4X
TPM1
TPM2
TPM4
TRAF5
TUBA1C
USP2
VCL
VIM
WDR1
WIPF1
ZC3H12A

Figure 2

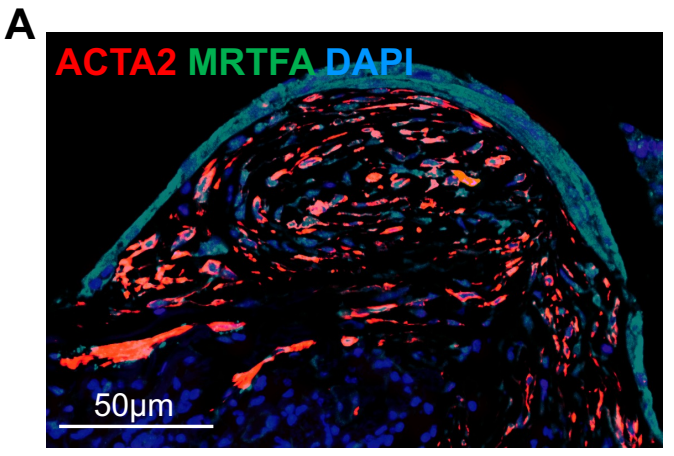
A
ACTA2 MRTFA DAPI
50μm

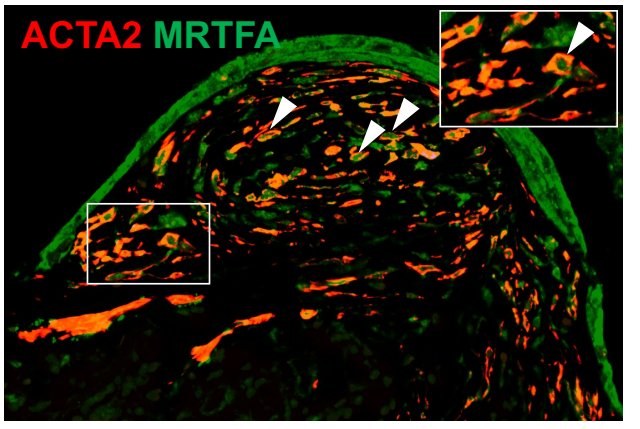
ACTA2 MRTFA

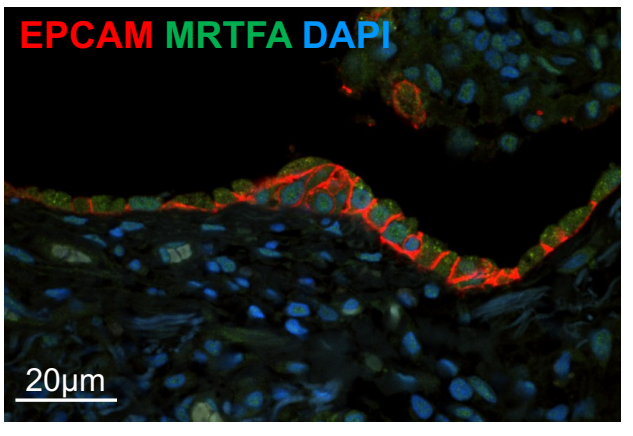
B
EPCAM MRTFA DAPI
20μm

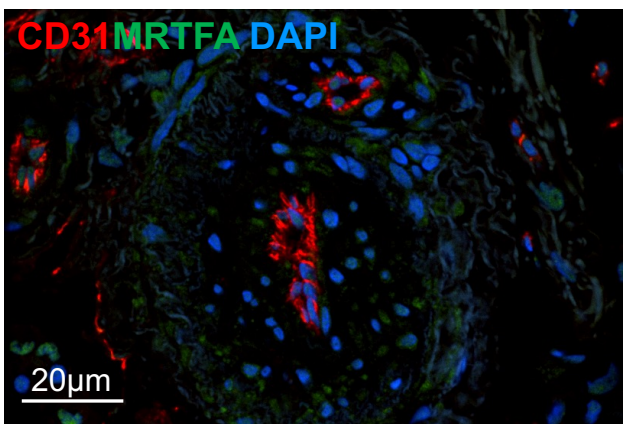
C
CD31MRTFA DAPI
20μm

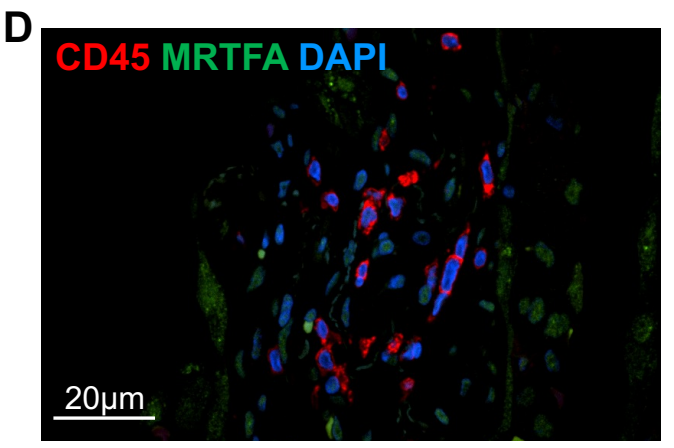
D
CD45 MRTFA DAPI
20μm

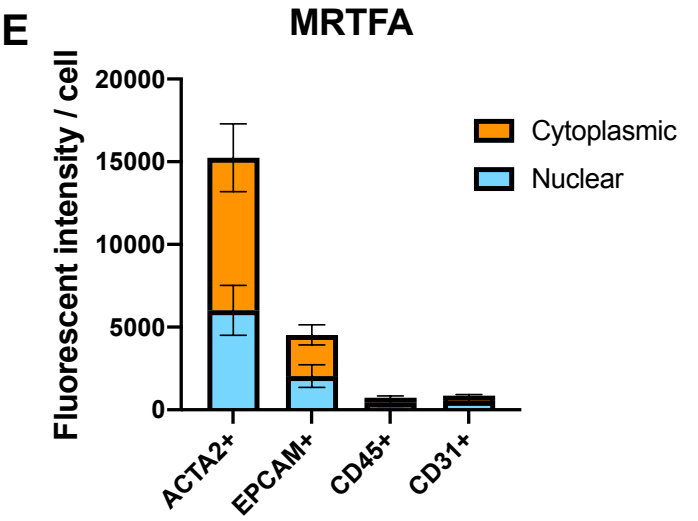
E
MRTFA
Fluorescent intensity / cell
20000
15000
10000
5000
0
Cytoplasmic
Nuclear
ACTA2+
EPCAM+
CD45+
CD31+

Figure 3

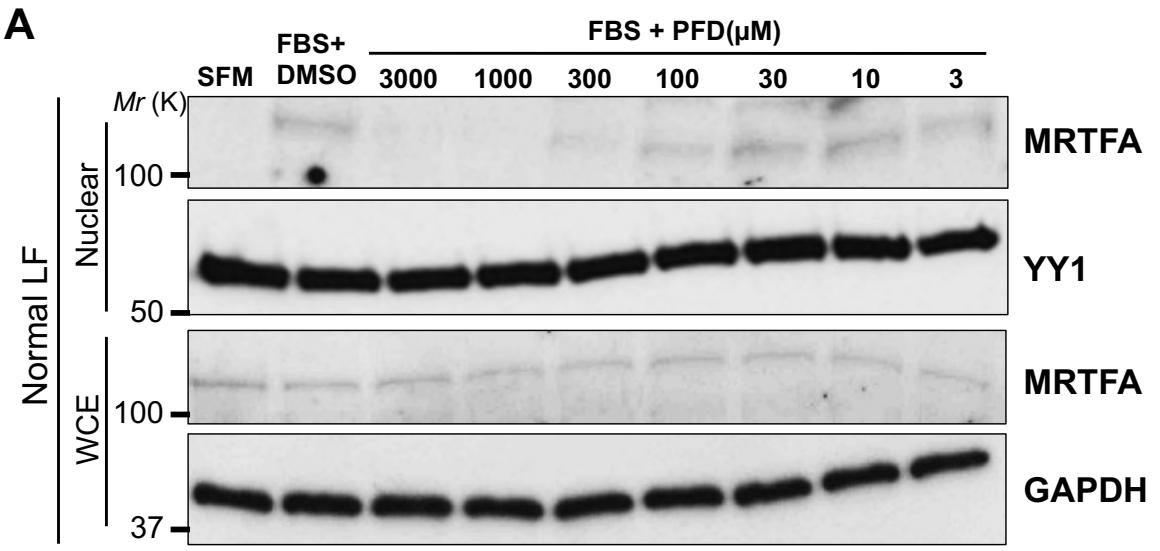

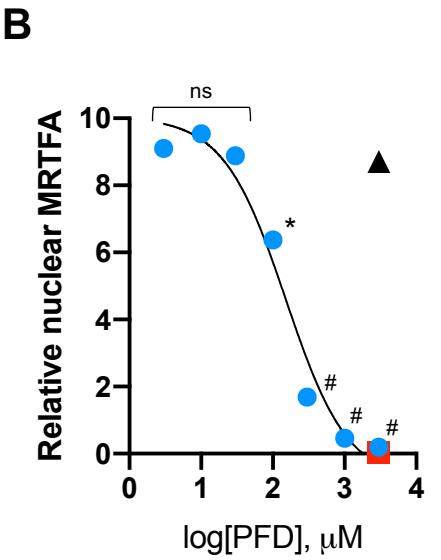

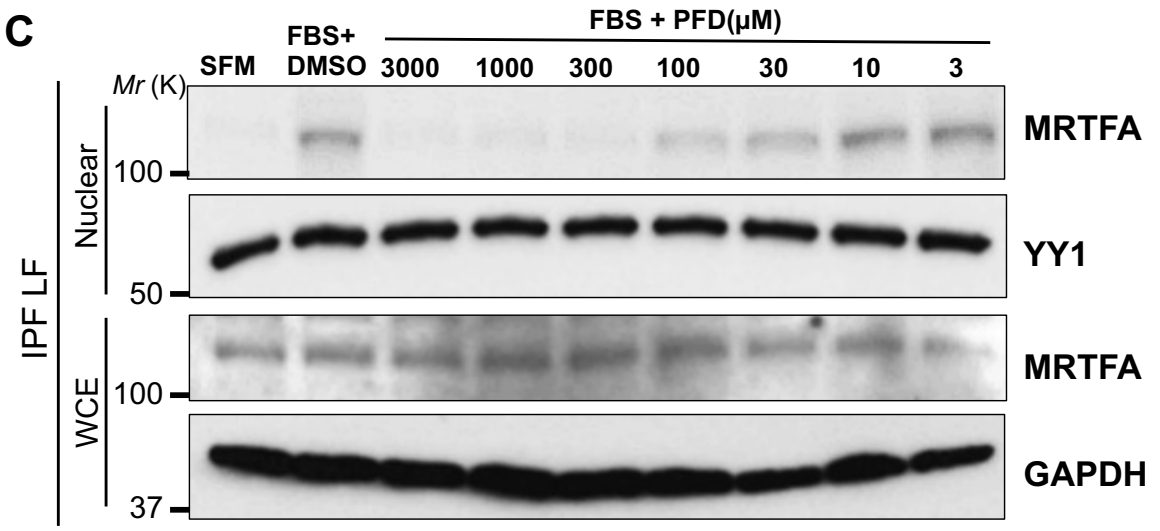

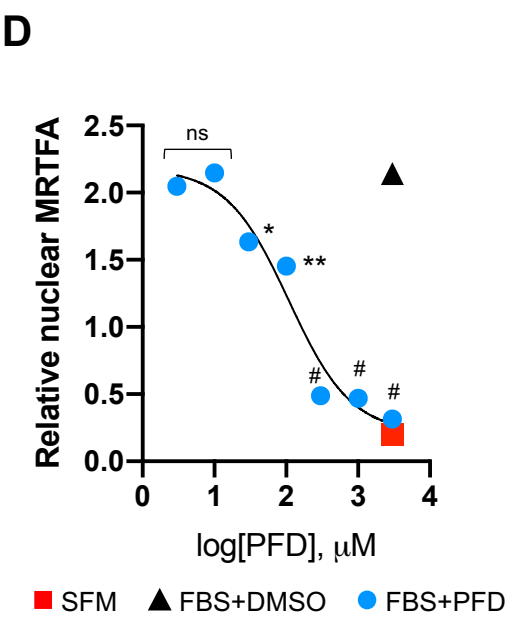

E

	Relative nuclear MRTFA	
	IC_{50} (μM) mean±S.D.	Max. Inh. (%) mean±S.D.
Normal LF	147 ± 7.07	97.33 ± 1.19
IPF LF	118 ± 12.02	91.85 ± 3.28

Figure 4

B

PFD suppressed genes (*p-adj.* <0.05)

Description	-Log10(q)
Biological Adhesion	19.56
Cell motility	13.49
Cell morphogenesis	13.61
Extracellular structure orgnization	12.03
Cell projection orgnization	10.24
Cytoskeleton orgnization	10.75
Actin filament based process	8.47
Regulation of cellular component movement	7.70

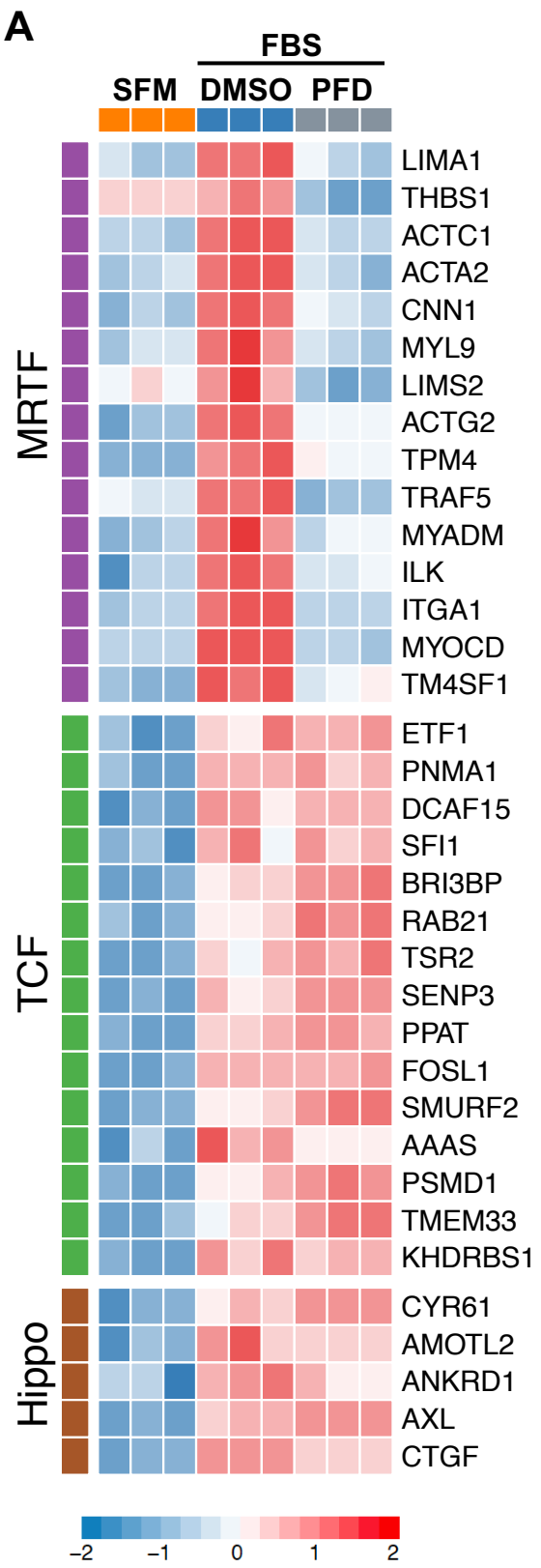

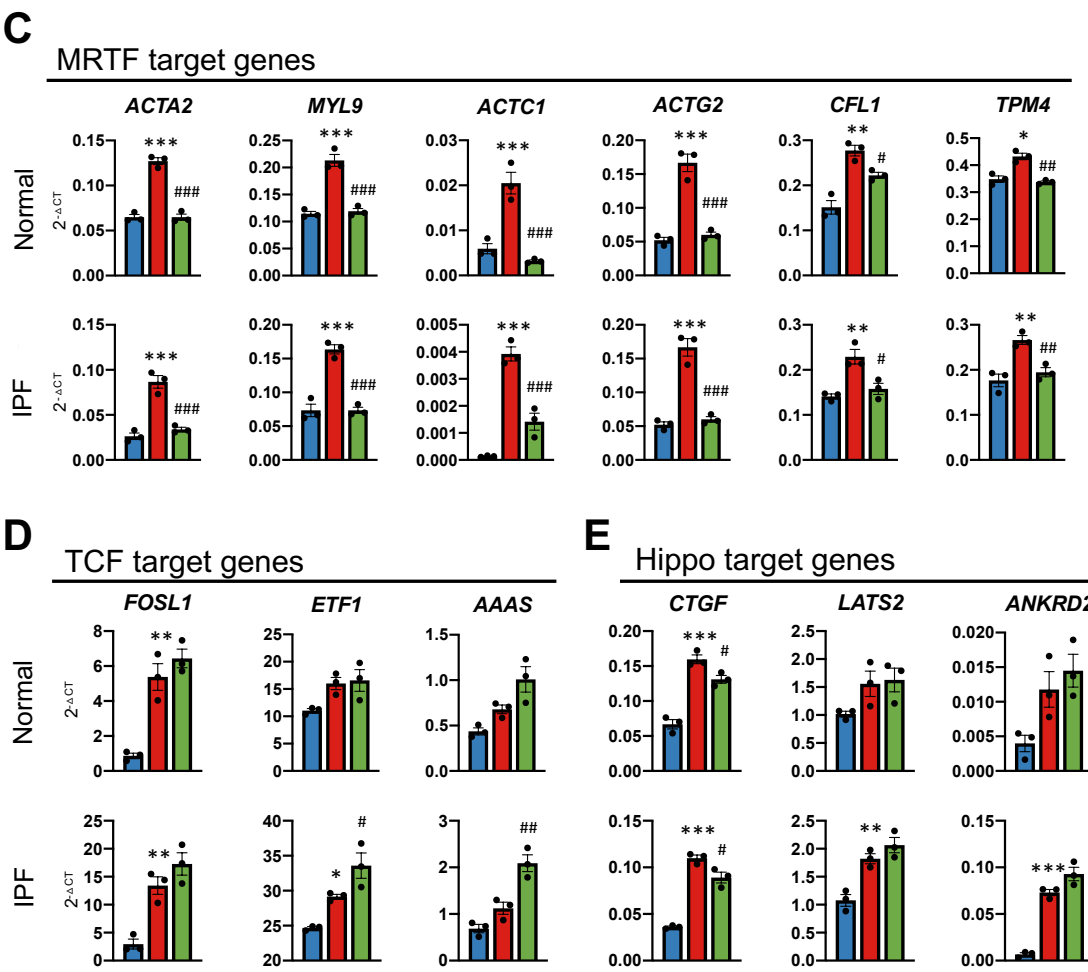

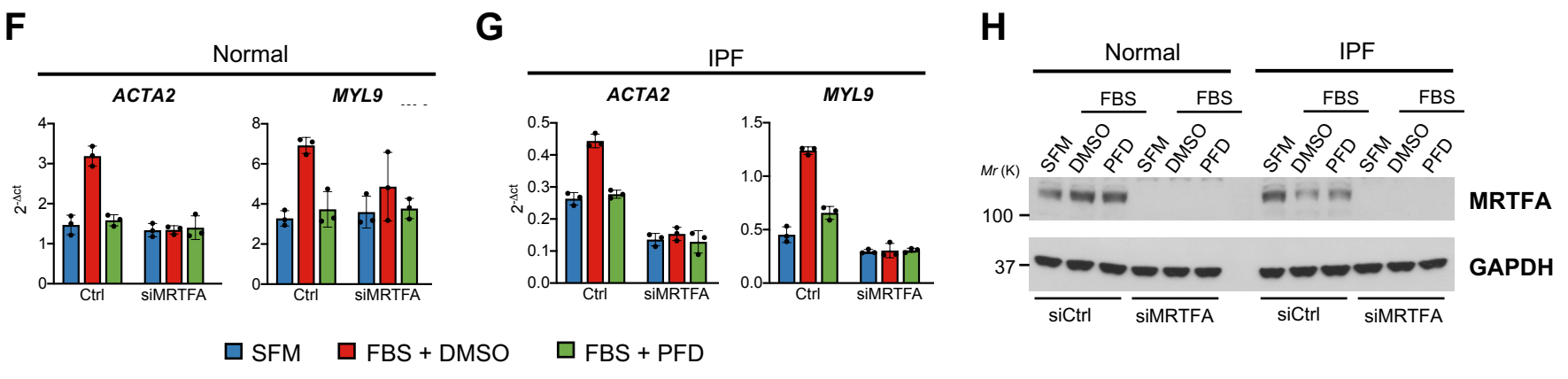

Figure 5

A

Normal LF

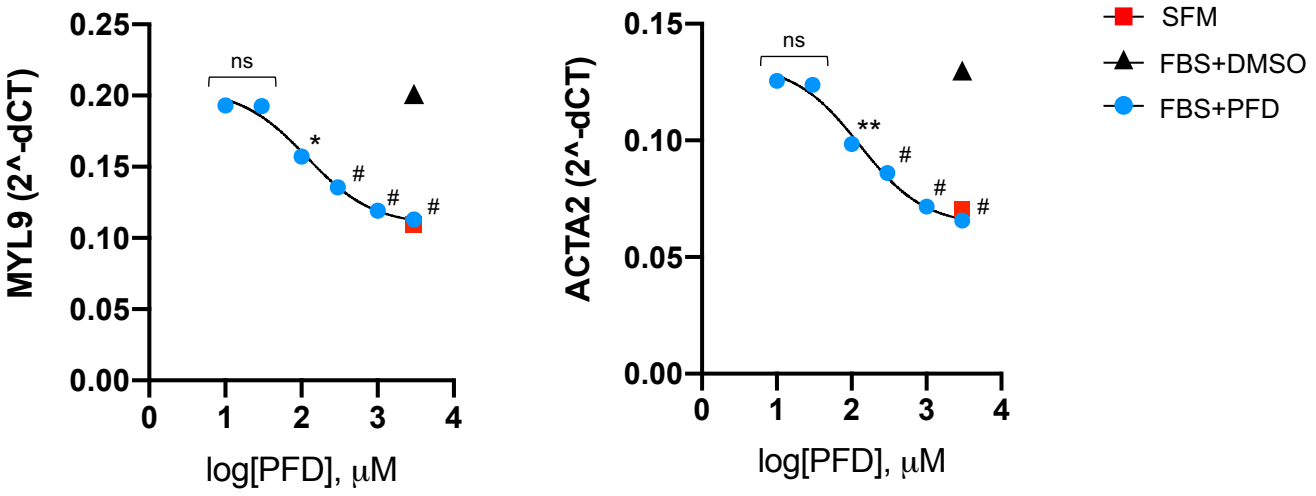

B

IPF LF

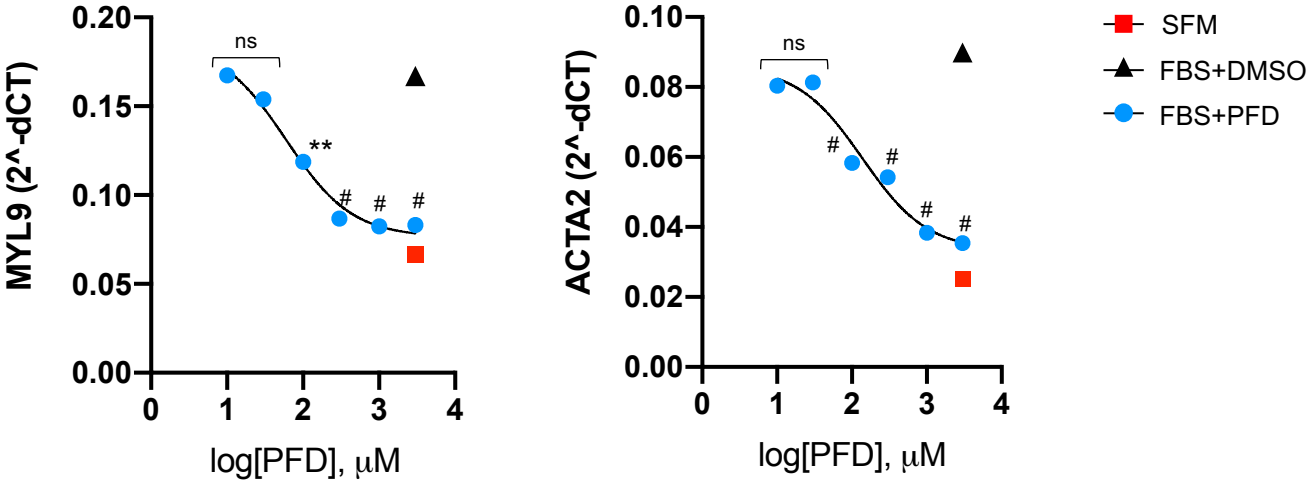

C

	IC_{50} (μM) mean±S.D.		Max. Inh. (%) mean±S.D.	
	MYL9	***ACTA2***	***MYL9***	***ACTA2***
Normal LF	78 ± 0.09	129 ± 0.35	97.88 ± 0.10	99.48 ± 0.11
IPF LF	66 ± 0.11	135 ± 0.06	93.68 ± 0.10	89.18 ± 0.08

Figure 6

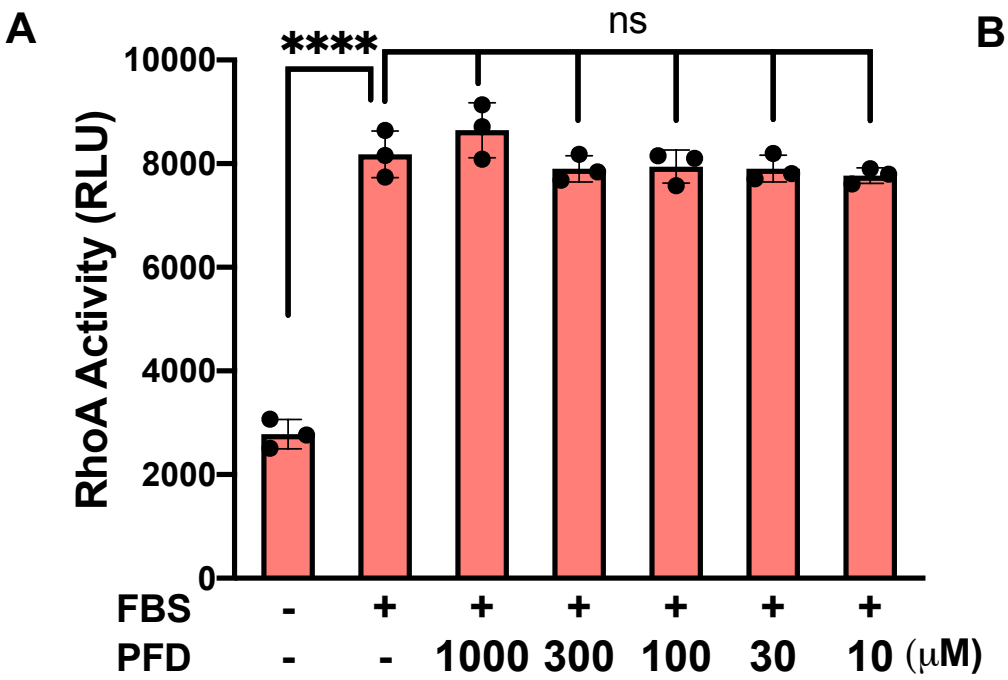
A
RhoA Activity (RLU)
10000
8000
6000
4000
2000
0
****
ns
FBS - + + + + + +
PFD - - 1000 300 100 30 10 (μM)

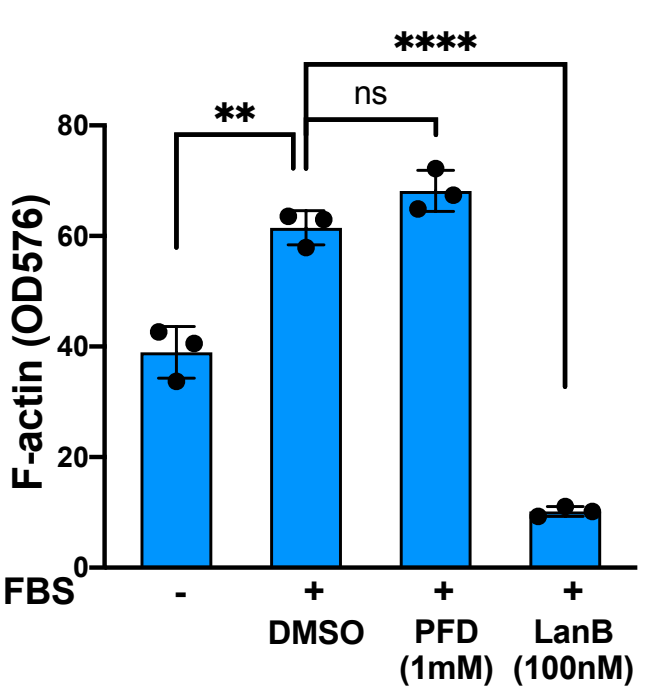
B
F-actin (OD576)
80
60
40
20
0
**
ns
****
FBS - + + +
DMSO
PFD (1mM)
LanB (100nM)

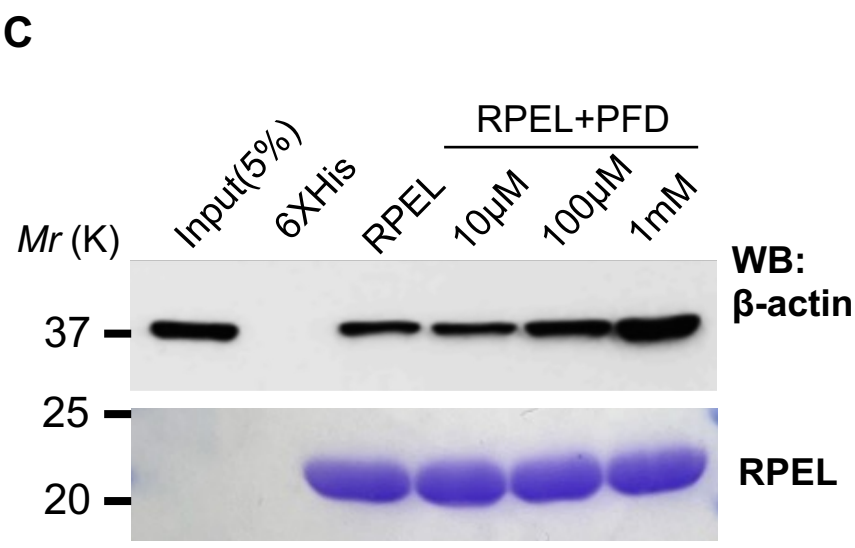
C
Mr (K)
Input(5%)
6XHis
RPEL
RPEL+PFD
10μM
100μM
1mM
WB:
β-actin
37
25
20
RPEL

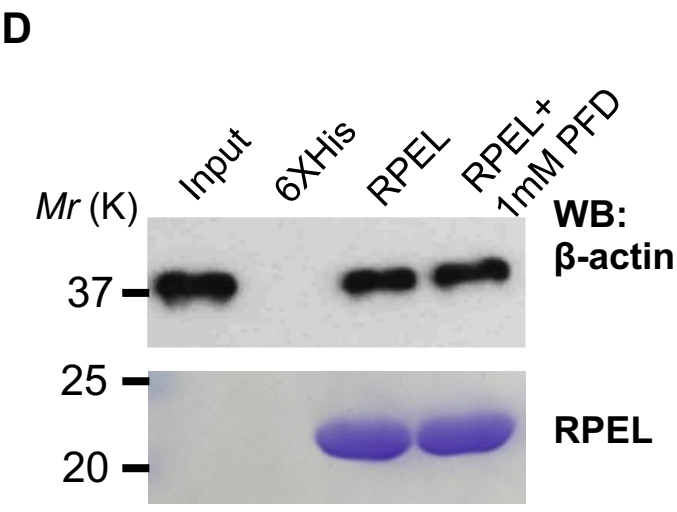
D
Mr (K)
Input
6XHis
RPEL
RPEL+
1mM PFD
WB:
β-actin
37
25
20
RPEL

Figure 7

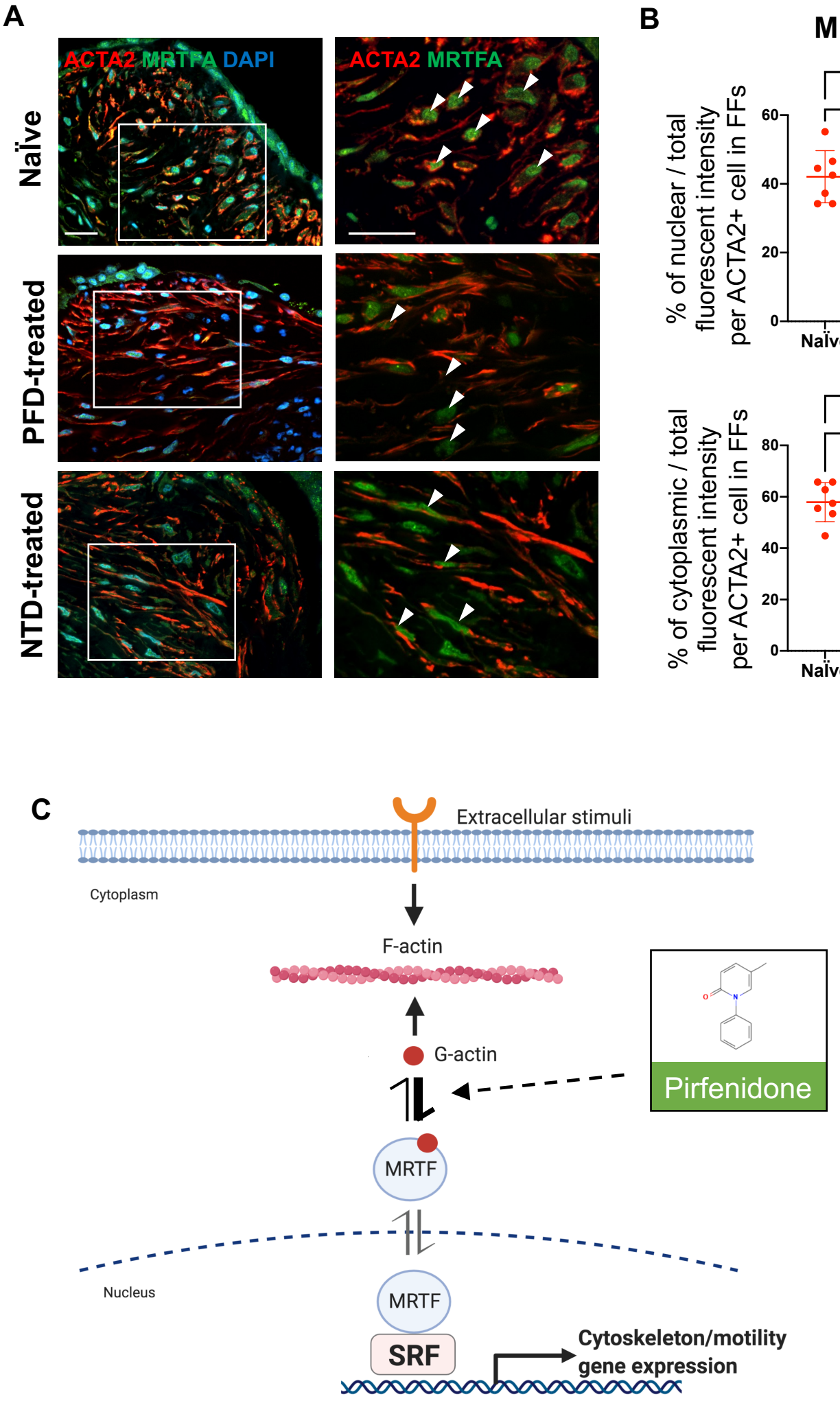
A
Naïve
PFD-treated
NTD-treated
ACTA2 MRTFA DAPI
ACTA2 MRTFA
B
MRTFA
ns
**
% of nuclear / total fluorescent intensity per ACTA2+ cell in FFs
60
40
20
0
Naïve PFD NTD
ns
**
% of cytoplasmic / total fluorescent intensity per ACTA2+ cell in FFs
80
60
40
20
0
Naïve PFD NTD
C
Extracellular stimuli
Cytoplasm
F-actin
G-actin
Pirfenidone
MRTF
Nucleus
MRTF
SRF
Cytoskeleton/motility gene expression

Figure S1

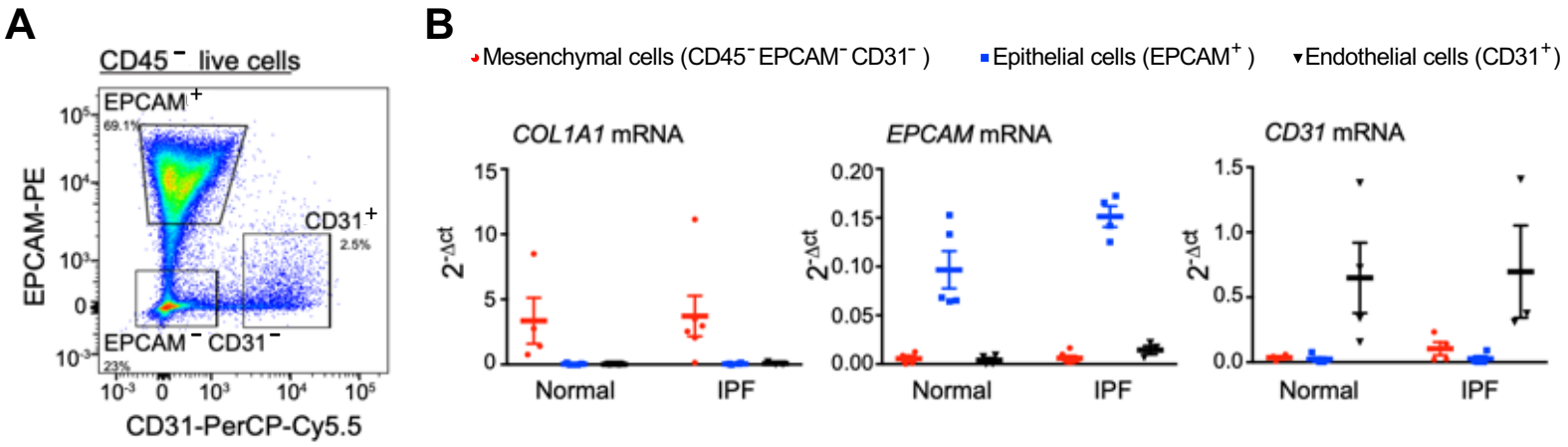
A
CD45⁻ live cells
EPCAM⁺
69.1%
CD31⁺
2.5%
EPCAM⁻ CD31⁻
23%
EPCAM-PE
CD31-PerCP-Cy5.5
B
Mesenchymal cells (CD45⁻EPCAM⁻CD31⁻)
Epithelial cells (EPCAM⁺)
Endothelial cells (CD31⁺)
COL1A1 mRNA
EPCAM mRNA
CD31 mRNA
2^-Δct
Normal
IPF

Figure S2

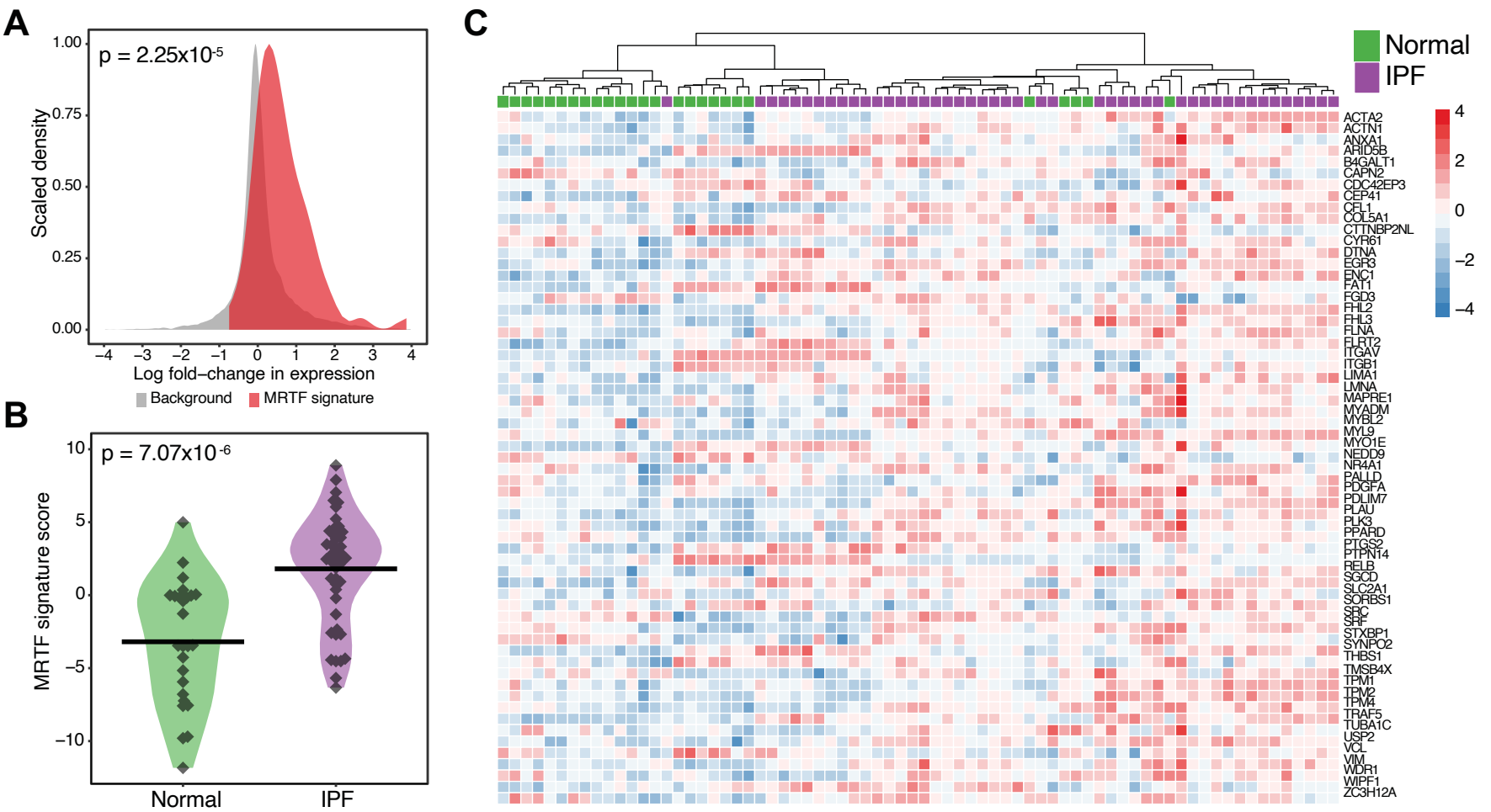
A
p = 2.25x10-5
Scaled density
1.00
0.75
0.50
0.25
0.00
−4 −3 −2 −1 0 1 2 3 4
Log fold−change in expression
Background
MRTF signature
B
p = 7.07x10-6
MRTF signature score
10
5
0
−5
−10
Normal
IPF
C
Normal
IPF
4
2
0
−2
−4
ACTA2
ACTN1
ANXA1
ARID5B
B4GALT1
CAPN2
CDC42EP3
CEP41
CFL1
COL5A1
CTTNBP2NL
CYR61
DTNA
EGR3
ENC1
FAT1
FGD3
FHL2
FHL3
FLNA
FLRT2
ITGAV
ITGB1
LIMA1
LMNA
MAPRE1
MYADM
MYBL2
MYL9
MYO1E
NEDD9
NR4A1
PALLD
PDGFA
PDLIM7
PLAU
PLK3
PPARD
PTGS2
PTPN14
RELB
SGCD
SLC2A1
SORBS1
SRC
SRF
STXBP1
SYNPO2
THBS1
TMSB4X
TPM1
TPM2
TPM4
TRAF5
TUBA1C
USP2
VCL
VIM
WDR1
WIPF1
ZC3H12A

Figure S3

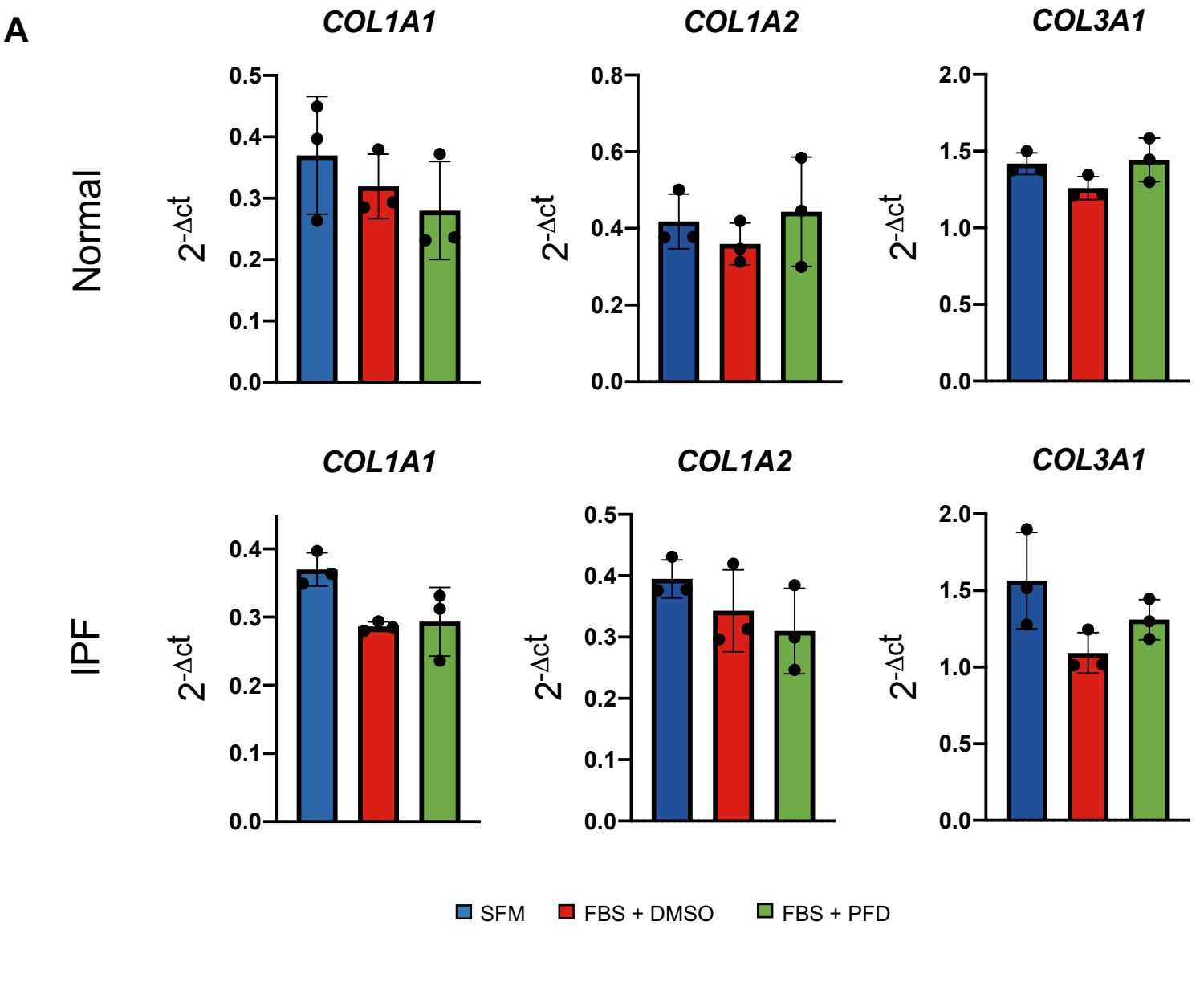
A
COL1A1
COL1A2
COL3A1
Normal
IPF
2-Δct
0.5
0.4
0.3
0.2
0.1
0.0
0.8
0.6
0.4
0.2
2.0
1.5
1.0
0.5
SFM
FBS + DMSO
FBS + PFD

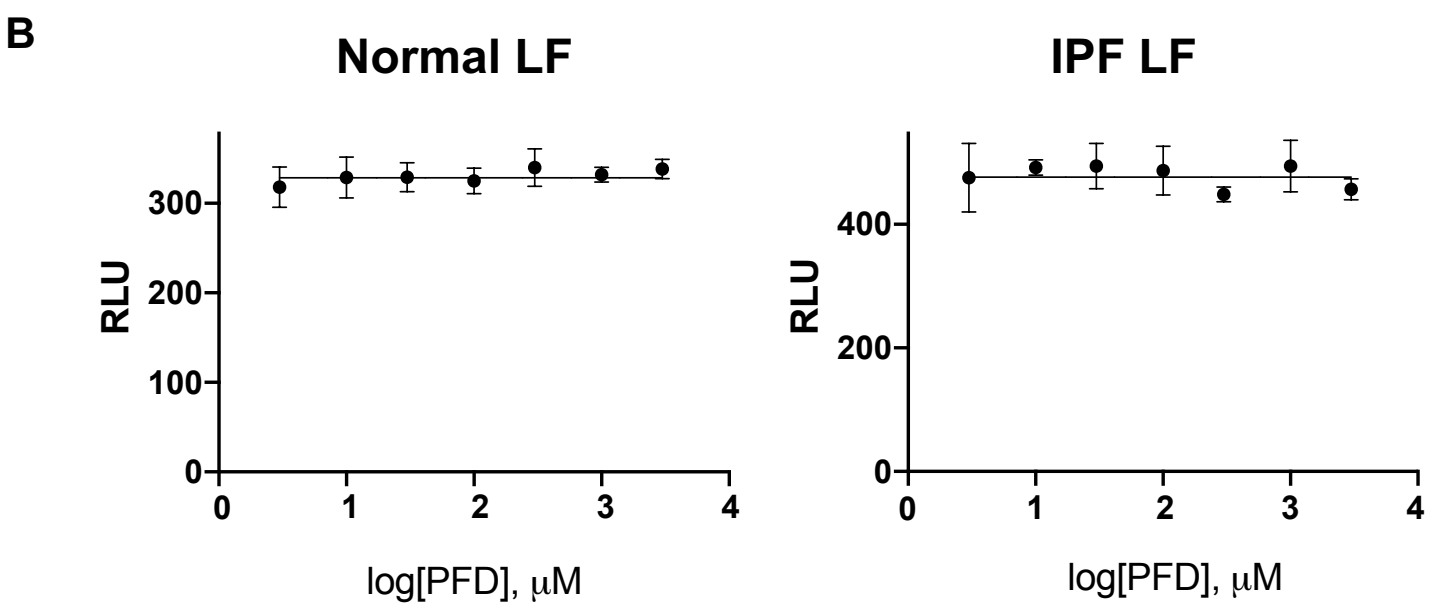
B
Normal LF
IPF LF
RLU
300
200
100
0
400
0
1
2
3
4
log[PFD], μM

Figure S4

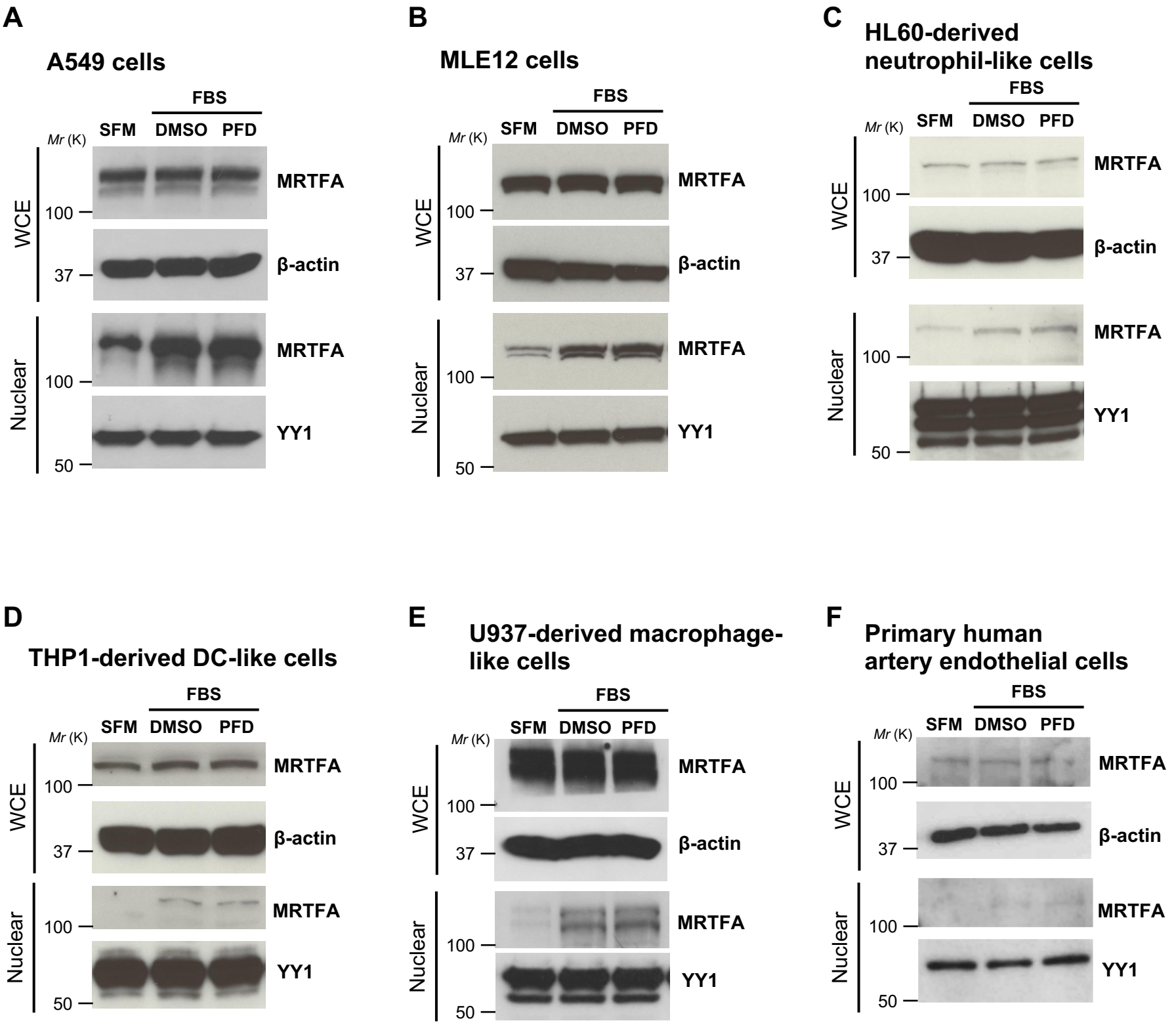
A
A549 cells
FBS
SFM
DMSO
PFD
Mr (K)
WCE
Nuclear
100
37
50
MRTFA
β-actin
YY1
B
MLE12 cells
C
HL60-derived neutrophil-like cells
D
THP1-derived DC-like cells
E
U937-derived macrophage-like cells
F
Primary human artery endothelial cells

Fig S5. Transcriptomics analyses of PFD effects on IPF LFs

A

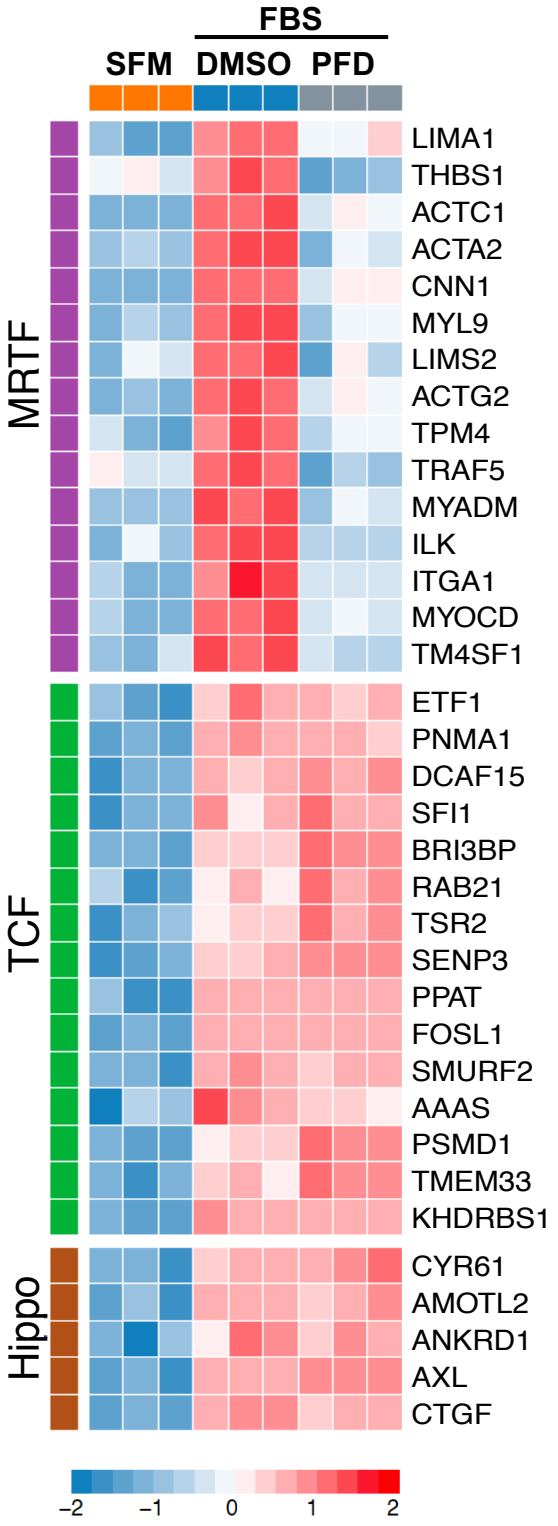

B

PFD suppressed genes (*p-adj.* <0.05)

Description	-Log10(q)
Cell motility	17.36
Biological Adhesion	15.98
Regulation of cellular component movement	13.65
Cell projection orgnization	12.34
Cell morphogenesis	12.10
Cytoskeleton orgnization	11.03
Actin filament based process	10.11
Extracellular structure orgnization	8.20

Figure S6

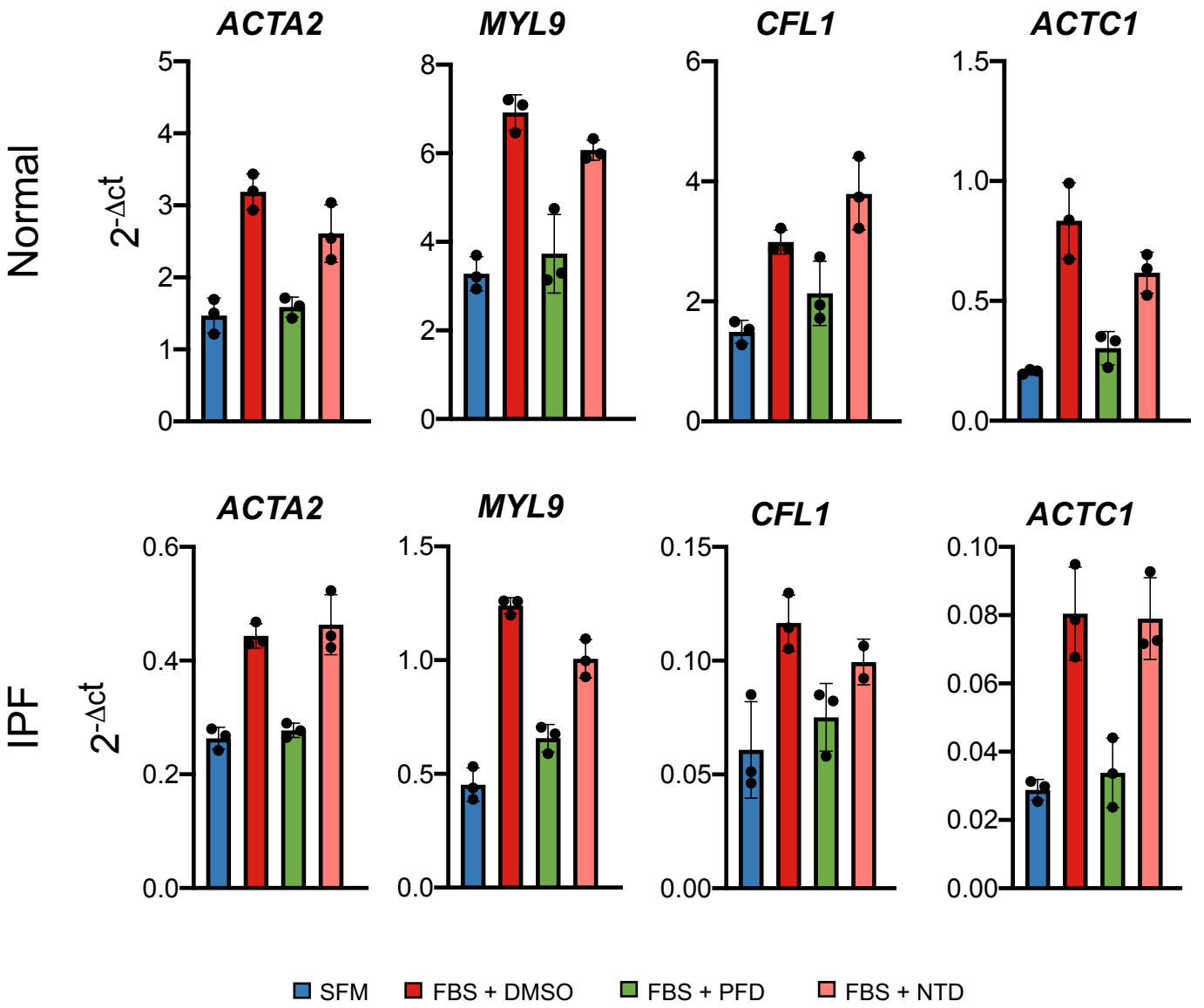
Normal
IPF
2-Δct
ACTA2
MYL9
CFL1
ACTC1
SFM
FBS + DMSO
FBS + PFD
FBS + NTD

Figure S7

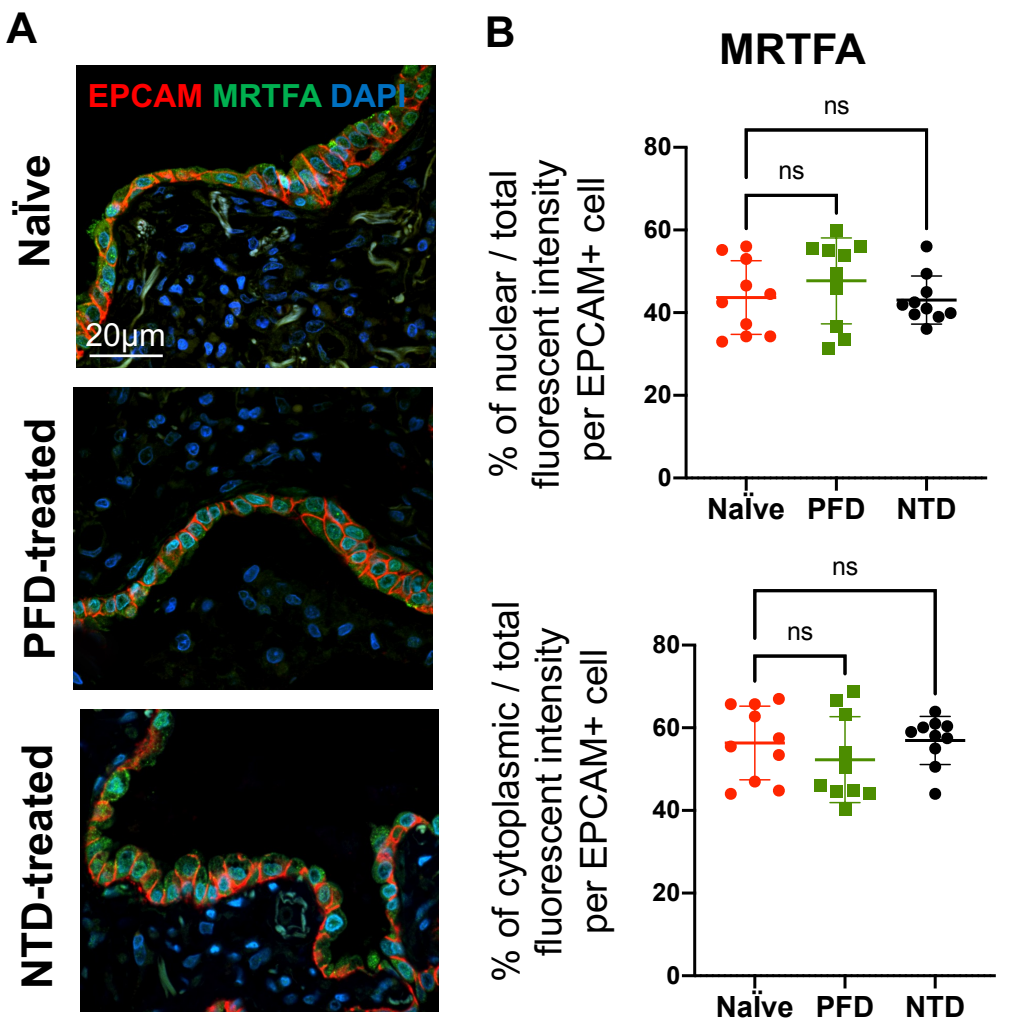
A
B
EPCAM MRTFA DAPI
Naïve
PFD-treated
NTD-treated
20μm
MRTFA
% of nuclear / total fluorescent intensity per EPCAM+ cell
% of cytoplasmic / total fluorescent intensity per EPCAM+ cell
ns
ns
0
20
40
60
80
Naïve
PFD
NTD

Table S1

Sample	Diagnosis	Gender	Age	Ethnicity	Drug therapy
N1	Normal	Male	61	Caucasian	NA
N2	Normal	Male	76	Caucasian	NA
N3	Normal	Male	34	Caucasian	NA
N4	Normal	Female	60	Caucasian	NA
I1	IPF	Male	63	Caucasian	None
I2	IPF	Male	68	Hispanic	Nintedanib
I3	IPF	Female	58	Caucasian	None
I4	IPF	Male	69	Caucasian	None
I5	IPF	Female	56	Caucasian	None
I6	IPF	Male	70	Caucasian	Pirfenidone
I7	IPF	Male	65	Caucasian	None
I8	IPF	Male	71	Caucasian	Nintedanib
I9	IPF	Male	59	Hispanic	None
I10	IPF	Female	66	Caucasian	Pirfenidone

Table S2

Primer	Sequence
hHPRT-F	CTCATGGACTGATTATGGACAGGAC
hHPRT-R	GCAGGTCAGCAAAGAACTTATAGCC
hCOL1A1-F	CAGACTGGCAACCTCAAGAA
hCOL1A1-R	CAGTGACGCTGTAGGTGAAG
hCOL1A2-F	GTTGCTGCTTGCAGTAACCTT
hCOL1A2-R	AGGGCCAAGTCCAACTCCTT
hCOL3A1-F	GGAGCTGGCTACTTCTCGC
hCOL3A1-R	GGGAACATCCTCCTTCAACAG
hCD31-F	AACAGTGTTGACATGAAGAGCC
hCD31-R	TGTAAAACAGCACGTCATCCTT
hEPCAM-F	AATCGTCAATGCCAGTGTACTT
hEPCAM-R	TCTCATCGCAGTCAGGATCATAA
hACTA2-F	GACCGAATGCAGAAGGAGAT
hACTA2-R	CACCGATCCAGACAGAGTATTT
hMYL9-F	TCTTCGCAATGTTTGACCAGT
hMYL9-R	GTTGAAAGCCTCCTTAAACTCCT
hACTA1-F	GGCATTCACGAGACCACCTAC
hACTA1-R	CGACATGACGTTGTTGGCATA
hACTG2-F	GCTGTAGCACCTGAAGAG
hACTG2-R	GAATGGCGACGTACATGGCA
hCFL1-F	GAGACCAAGGAG AGCAAGAAG
hCFL1-R	GTCCTTGGAGCTGGCATAAA
hTPM4-F	CTGAGACCCGTGCTGAAT TT
hTPM4-R	AGCCCACGTTCTCTTCTTTG
hCTGF-F	GCCCAGACCCAACTATGATTAG
hCTGF-R	GGAGGCGTTGTCATTGGTAA
hFOSL1-F	CAGGCGGAGACTGACAAACTG
hFOSL1-R	TCCTTCCGGGATTTTGCAGAT
hAAAS-F	GGCCTTTTTGGGGTGCTAAAT
hAAAS-R	TGGGCAAATTCAGCGATCAGA
hETF1-F	ATACAGAGGCTCTTACAGCACT
hETF1-R	AATTTGTGCAGGACTTCTCTTGT
hANKRD1-F	AGTAGAGGAACTGGTCACTGG
hANKRD1-R	TGTTTCTCGCTTTTCCACTGTT
hAXL-F	CCGTGGACCTACTCTGGCT
hAXL-R	CCTTGGCGTTATGGGCTTC